

Canonical Quantization of Cylindrical Waveguides: A Gauge-Based Approach

Alexandre Delattre¹ and Eddy Collin^{1,*}

¹*Institut Néel, CNRS/UGA, 38042 Grenoble, France*

(Dated: February 5, 2026)

Abstract

We present a canonical quantization of electromagnetic modes in cylindrical waveguides, extending a gauge-based formalism previously developed for Cartesian geometries [1]. By introducing the two field quadratures X, Y of TEM (transverse electric-magnetic), but also of TM (transverse magnetic) and TE (transverse electric) traveling modes, we identify for each a characteristic one-dimensional scalar field (a *generalized flux* φ) governed by a Klein-Gordon type equation. The associated Hamiltonian is derived explicitly from Maxwell's equations, allowing the construction of bosonic ladder operators. The generalized flux is directly deduced from the electromagnetic potentials \mathbf{A}, V by a proper *gauge choice*, generalizing Devoret's approach [2]. Our analysis unifies the treatment of cylindrical and Cartesian guided modes under a consistent and generic framework, ensuring both theoretical insight and experimental relevance. We derive mode-specific capacitance and inductance from the field profiles and express voltage and current in terms of the canonical field variables. Measurable quantities are therefore properly defined from the mode quantum operators, especially for the non-trivial TM and TE ones. The formalism shall extend in future works to any other type of waveguides, especially on-chip coplanar geometries particularly relevant to quantum technologies.

* eddy.collin@neel.cnrs.fr

CONTENTS

I. Introduction	3
II. Prelude on Bessel functions	4
III. Basics: Maxwell's Equations in Cylindrical Geometry	6
A. Maxwell's equations in an ideal material	6
B. Boundary conditions in cylindrical geometry	7
C. Factorized form of the fields	7
D. Coaxial waveguide	9
1. TEM modes	9
2. TM modes	9
3. TE modes	10
4. Comparison with Cartesian geometry	12
E. Hollow cylindrical waveguide	13
1. TM modes	13
2. TE modes	15
IV. Charges, currents, and constants of motion in cylindrical geometry	16
A. Constants of motion of the electromagnetic field	16
B. Generalized fluxes	17
C. Coaxial waveguide	18
1. TEM modes	18
2. TM modes	19
3. TE modes	20
D. Hollow cylindrical waveguide	24
1. TM modes	24
2. TE modes	25
V. Electromagnetic gauge	27
A. Coaxial waveguide	29
1. TEM modes	29
2. TM modes	29

3. TE modes	31
B. Hollow cylindrical waveguide	34
1. TM modes	35
2. TE modes	36
C. Gauge fixing strategies: Cartesian vs cylindrical geometries	37
VI. Field quantization	42
VII. Conclusion	45
Acknowledgements	46
Data availability	46
Conflict of interest	46
References	46

I. INTRODUCTION

The transfer of quantum information via light fields (let them be lasers or microwave signals) is at the heart of modern quantum technologies. Building on the original developments of quantum electrodynamics (QED) [3–6], the circuit-based approach of Devoret and collaborators (cQED) [2, 7, 8] identified generalized variables (flux and charge) that enabled a rigorous Hamiltonian formulation of superconducting quantum circuits. This formalism has been instrumental in the rise of cQED, where superconducting qubits interact with quantized microwave modes [9–11], as well as in the design of modern nonlinear quantum devices such as traveling-wave parametric amplifiers (TWPAs) [12, 13].

While the explicit quantization of all types of waves (TEM, TM and TE) in Cartesian waveguides has been recently developed [1], the extension to cylindrical geometries remained to be performed. These are indeed ubiquitous in both classical microwave engineering [14–16] and modern quantum platforms. Cylindrical cavities and waveguides are routinely used in particle accelerators [17], cavity optomechanics (in its microwave version) [18, 19], quantum hybrid systems [20], and topological photonics [21].

In this work, we extend the canonical quantization framework of Ref. [1] to cylindrical waveguides. Starting from Maxwell's equations for electric \mathbf{E} and magnetic \mathbf{B} fields in cylindrical coordinates, we derive explicit modal profiles for TEM, TM and TE modes, and express all the fields' characteristics in terms of a generalized flux variable φ , in analogy with Devoret's prescription, imposing a proper electromagnetic gauge to the potentials \mathbf{A} , V . Our modeling emphasizes the universality of the canonical formalism, leading to a one-to-one correspondence between the Cartesian treatment and the cylindrical one. Especially, the notion of *virtual electrodes* is invoked, and the specificity of the corresponding gauge is discussed. With the identification of proper mode-dependent voltage and current quantities, the mapping to transmission line theory (with the definition of effective capacitance and inductance per unit length) can be naturally obtained for *any* type of waves. To date, this is performed rigorously only for the TEM ones [6, 16], and shall be developed in oncoming articles.

II. PRELUDE ON BESSEL FUNCTIONS

We give here the basic mathematical tools specific to the cylindrical symmetry, for the interested reader willing to redo the calculations. The analysis of electromagnetic modes in cylindrical geometries [16] naturally leads to the *Bessel differential equation* [22, 23]:

$$x^2 \frac{d^2 y}{dx^2} + x \frac{dy}{dx} + (x^2 - n^2) y = 0, \quad (1)$$

where $n \in \mathbb{Z}$ is the azimuthal index, arising from the separation of variables in the angular coordinate θ and radial coordinate $r \geq 0$; $x = k_c r$ with k_c a positive real number to be defined (see below). The two linearly independent solutions of Eq. (1) are the *Bessel functions of the first kind* $J_n(x)$ and the *Bessel functions of the second kind* $Y_n(x)$, also known as Neumann functions. Their mathematical properties are extensively documented in the literature [22, 23], and their application is standard in many areas of physics [24].

The function $J_n(x)$ is finite at $x = 0$, whereas $Y_n(x)$ diverges as $x \rightarrow 0$; both verify $J_{-n}(x) = (-1)^n J_n(x)$ and $Y_{-n}(x) = (-1)^n Y_n(x)$ for integer $n \geq 0$. For waveguides that include the axis $r = 0$ (namely hollow cylinders), regularity of the physical fields requires discarding $Y_n(x)$ in \mathbf{E}, \mathbf{B} field expressions. In contrast, for coaxial waveguides the origin is excluded from the domain and both J_n and Y_n are admissible solutions. In such cases, the

generic radial profile takes the form:

$$R(r) = A J_n(k_c r) + B Y_n(k_c r), \quad (2)$$

with coefficients A and B determined (as well as k_c) by the electromagnetic boundary conditions on the conducting surfaces at $r = a$ and $r = b$, see Fig. 1.

Several identities involving J_n and Y_n are of practical importance in mode analysis. The *Wronskian identity*:

$$J_n(x)Y'_n(x) - J'_n(x)Y_n(x) = \frac{2}{\pi x}, \quad (3)$$

is frequently used in normalization procedures. The *derivative recurrence relations*:

$$J'_n(x) = \frac{1}{2} [J_{n-1}(x) - J_{n+1}(x)], \quad Y'_n(x) = \frac{1}{2} [Y_{n-1}(x) - Y_{n+1}(x)], \quad (4)$$

allow one to express radial derivatives directly in terms of Bessel functions of adjacent orders. J_n and Y_n play here roles analogous to the transverse sine and cosine components found in Cartesian geometries [1]. In the following sections, these functions will serve as the building blocks for the radial profiles of TM and TE modes in coaxial waveguides and hollow cylinders, with the specific combination in Eq. (2) fixed by the mode type and boundary conditions [16].

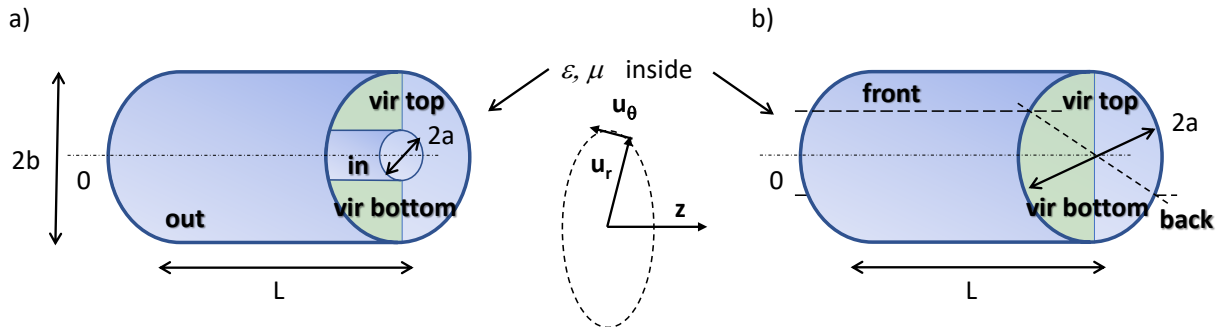


FIG. 1. Geometries with cylindrical symmetry. a) coaxial line. b) hollow cylinder. The axes corresponding to the coordinate system r, θ, z are displayed. Real electrodes are shown in blue (*in* and *out* labels for coaxial, and *front*, *back* for hollow pipe). The *virtual electrodes* (labeled *vir top* and *vir bottom*) are shown in green. See text for details.

III. BASICS: MAXWELL'S EQUATIONS IN CYLINDRICAL GEOMETRY

We consider two types of guides preserving the cylindrical symmetry with transverse coordinates $\{r, \theta\}$, see Fig. 1. We assume that they are filled with a lossless, homogeneous, and isotropic medium of permittivity ϵ and permeability μ , over a length L .

The coaxial line consists of *two* perfectly conducting concentric cylindrical surfaces of inner radius $r = a$ and outer radius $r = b$ (with $b > a$). The z -axis is aligned with the common axis of both conductors. The inner conductor properties are designated by a label *in*, while the outer ones take an *out*.

The other type of guide possesses a *single* electrode: it consists in a cylinder of radius a , oriented along the z -axis. As for the coaxial line, the surface at $r = a$ is assumed to be a perfect electric conductor. We attach to the properties related to this electrode the labels *front* and *back*, designating two radially opposite points of the surface, for any $\theta, \theta + \pi$. This corresponds here to the two sets of equivalent electrodes defined in the Cartesian case (*top, bottom* and *left, right* respectively) [1], but preserving the cylindrical symmetry.

Treating Cartesian and cylindrical geometries within the same formalism is indeed particularly enlightening: it enables to reveal the topological equivalence between these guided modes, and also to refine our understanding of *virtual electrodes*, as introduced in Ref. [1]. They correspond to diameter planes, with *vir top* designating the top part of the diameter and *vir bottom* the other side (see Fig. 1). These are defined for specific TE modes only, see discussion below. We demonstrate that the concepts introduced in the (simpler) Cartesian geometry do apply here, when properly adapted, especially regarding the gauge choice.

A. Maxwell's equations in an ideal material

The electric and magnetic fields \mathbf{E} (V/m) and \mathbf{B} (T) obey the well-known Maxwell equations:

$$\nabla \cdot \mathbf{E}(r, \theta, z, t) = 0, \quad (5)$$

$$\nabla \cdot \mathbf{B}(r, \theta, z, t) = 0, \quad (6)$$

$$\nabla \times \mathbf{E}(r, \theta, z, t) = -\frac{\partial \mathbf{B}(r, \theta, z, t)}{\partial t}, \quad (7)$$

$$\nabla \times \mathbf{B}(r, \theta, z, t) = \frac{1}{c^2} \frac{\partial \mathbf{E}(r, \theta, z, t)}{\partial t}, \quad (8)$$

with $c = 1/\sqrt{\mu\epsilon}$ the speed of light in the chosen dielectric (ϵ permittivity, μ permeability). Since we aim at describing quantum information transfer in the low-energy QED regime, these linear relations are all we need: we assume that the material is *ideal*, with no nonlinear properties. Dielectric losses are also neglected, as already mentioned.

B. Boundary conditions in cylindrical geometry

In cylindrical coordinates (r, θ, z) , the conductor walls of our configurations are located at $r = a$ and $r = b$, with a normal unit vector given by $\mathbf{n} = \pm\mathbf{u}_r$ depending on the orientation of the surface (+ for the inner conductor of the coaxial guide, and – for the outer one or for the cylinder). The generic electromagnetic boundary conditions on the electrodes read:

$$\mathbf{n} \cdot \mathbf{E}(r = \{a; b\}, \theta, z, t) = +\frac{\sigma_s(\theta, z, t)}{\epsilon}, \quad (9)$$

$$\mathbf{n} \cdot \mathbf{B}(r = \{a; b\}, \theta, z, t) = 0, \quad (10)$$

$$\mathbf{n} \times \mathbf{E}(r = \{a; b\}, \theta, z, t) = 0, \quad (11)$$

$$\mathbf{n} \times \mathbf{B}(r = \{a; b\}, \theta, z, t) = +\mu \mathbf{j}_s(\theta, z, t), \quad (12)$$

where $\sigma_s(\theta, z, t)$ is the surface charge density and $\mathbf{j}_s(\theta, z, t)$ is the surface current density on the wall. In the following sections, we will use these electromagnetic boundary conditions to determine the mode families supported by the guide. Our only physical assumption is that the electrodes are made of ideal conductors, so that losses can be neglected. But note that nothing is specified about the microscopic nature of the charges (free electrons or Cooper pairs): only their coupling to the electromagnetic field is relevant. The same boundary conditions Eqs. (9-12) shall apply to *virtual electrodes* (choosing $\mathbf{n} = \pm\mathbf{u}_\theta$ for normal vector, and $a < r < b$ or $0 < r < a$ depending on the configuration), as discussed in the following.

C. Factorized form of the fields

The factorized representation of the fields applies to all guided modal families supported by the geometry under consideration. Considering traveling wave solutions, we therefore

define, following conventions from Ref. [1] :

$$f(z, t) = X \cos(\omega t - \beta z + \phi_0) + Y \sin(\omega t - \beta z + \phi_0),$$

$$\tilde{f}(z, t) = X \sin(\omega t - \beta z + \phi_0) - Y \cos(\omega t - \beta z + \phi_0),$$

with $\beta = 2\pi l/L$ the wavevector (we use periodic boundaries, $l \in \mathbb{Z}^*$), $\omega = ck$ the angular frequency ($k > 0$), and ϕ_0 an arbitrary phase linked to the t, z origins. The phase velocity reads $v_\phi = ck/|\beta|$. X and Y are the two field quadratures (no units), which quantify the state of the microwave field. The electromagnetic field components can then be expressed as:

$$E_r(r, \theta, z, t) = E_m g_{E_r}(r, \theta) f(z, t), \quad (13)$$

$$E_\theta(r, \theta, z, t) = E_m g_{E_\theta}(r, \theta) f(z, t), \quad (14)$$

$$E_z(r, \theta, z, t) = E_m g_{E_z}(r, \theta) \tilde{f}(z, t), \quad (15)$$

$$B_r(r, \theta, z, t) = B_m g_{B_r}(r, \theta) f(z, t), \quad (16)$$

$$B_\theta(r, \theta, z, t) = B_m g_{B_\theta}(r, \theta) f(z, t), \quad (17)$$

$$B_z(r, \theta, z, t) = B_m g_{B_z}(r, \theta) \tilde{f}(z, t), \quad (18)$$

where $E_m > 0$ sets the electric field amplitude, and $B_m = E_m/c$ the magnetic field amplitude. Note that g_{E_i} and g_{B_i} are *dimensionless*: these functions are the normalized transverse modal profiles, to be determined for each configuration by solving Maxwell's equations with the boundary conditions Eqs. (9)–(12). In the next sections, this is performed explicitly for the coaxial structure (leading to the well known TEM, TM, TE families), and then for the hollow cylinder (TM and TE), reformulating (for our purpose) results found in the literature [16]. The longitudinal envelopes verify, as in the Cartesian formulation:

$$\frac{\partial f}{\partial t} = -\omega \tilde{f}, \quad \frac{\partial f}{\partial z} = +\beta \tilde{f}, \quad \frac{\partial \tilde{f}}{\partial t} = +\omega f, \quad \frac{\partial \tilde{f}}{\partial z} = -\beta f, \quad (19)$$

which are identities used to simplify the calculations. We take arbitrarily the sign convention for the transverse profiles such that the charge amplitude on the $r = a$ conductor (inner one for the coaxial line, or confining cylinder for the other type of guide) is positive, with a normalization such that the electric field amplitude verifies $|g_{E_r}(r = a)| = 1$ on this electrode (regardless of the azimuthal cos or sin dependence when it exists; see below). The case of virtual electrodes shall be specifically discussed when necessary.

D. Coaxial waveguide

Three distinct families of propagating waves exist in a coaxial line [16]. They are in direct correspondence with the ones found for electromagnetic signals propagating between two plates [1]. These are presented in the following.

1. TEM modes

The TEM family is the simplest one, and it satisfies:

$$k = |\beta|, \quad E_z = 0, \quad B_z = 0, \quad (20)$$

with no longitudinal components, and a linear dispersion relation (thus $v_\phi = c$). The dimensionless profiles are given in Tab. I below.

TABLE I. Dimensionless modal profiles for the TEM modes in a coaxial waveguide.

Function	Expression
$g_{E_r}(r)$	$= \frac{a}{r}$
$g_{E_\theta}(r)$	$= 0$
$g_{E_z}(r)$	$= 0$
$g_{B_r}(r)$	$= 0$
$g_{B_\theta}(r)$	$= \frac{a}{r} \text{sign}(\beta)$
$g_{B_z}(r)$	$= 0$

The **E** field is radial, and the **B** field tangential [16]. The wavevector β characterizes each propagating mode.

2. TM modes

TM modes are defined by $B_z = 0$ and $E_z \neq 0$. The boundary condition on the two electrodes impose ($n \geq 0$):

$$J_n(k_c a) Y_n(k_c b) - J_n(k_c b) Y_n(k_c a) = 0, \quad (21)$$

from which one obtains the dispersion relation $k^2 = k_c^2 + \beta^2$, with $\omega_c = c k_c$ the cutoff frequency below which the TM waves cannot propagate. Eq. (21) leads to a discrete set of solutions for k_c , that we index by $m > 0$. Each propagating mode is thus characterized by *two* indexes n, m (while in the parallel plate case, only one was enough [1]), plus a wavevector β . The dimensionless profiles are given in Tab. II, with θ_0 an arbitrary choice for the $\theta = 0$ reference.

TABLE II. Dimensionless modal profiles for $\text{TM}_{n,m}$ in a coaxial waveguide ($n \geq 0, m > 0$). We defined $A_{n,m} = (4\beta)/[\pi k_c^2 a Y_n(k_c a)]$.

Function	Expression
$g_{E_r}(r, \theta)$	$= -\frac{\beta}{k_c A_{n,m}} \left[J_{n-1}(k_c r) - J_{n+1}(k_c r) - \frac{J_n(k_c a)}{Y_n(k_c a)} (Y_{n-1}(k_c r) - Y_{n+1}(k_c r)) \right] \cos[n(\theta - \theta_0)]$
$g_{E_\theta}(r, \theta)$	$= +\frac{2\beta n}{k_c^2 r A_{n,m}} \left[J_n(k_c r) - \frac{J_n(k_c a)}{Y_n(k_c a)} Y_n(k_c r) \right] \sin[n(\theta - \theta_0)]$
$g_{E_z}(r, \theta)$	$= +\frac{2}{A_{n,m}} \left[J_n(k_c r) - \frac{J_n(k_c a)}{Y_n(k_c a)} Y_n(k_c r) \right] \cos[n(\theta - \theta_0)]$
$g_{B_r}(r, \theta)$	$= -\frac{2k n}{k_c^2 r A_{n,m}} \left[J_n(k_c r) - \frac{J_n(k_c a)}{Y_n(k_c a)} Y_n(k_c r) \right] \sin[n(\theta - \theta_0)]$
$g_{B_\theta}(r, \theta)$	$= -\frac{k}{k_c A_{n,m}} \left[J_{n-1}(k_c r) - J_{n+1}(k_c r) - \frac{J_n(k_c a)}{Y_n(k_c a)} (Y_{n-1}(k_c r) - Y_{n+1}(k_c r)) \right] \cos[n(\theta - \theta_0)]$
$g_{B_z}(r, \theta)$	$= 0$

The **E** and **B** fields have thus *both* a specific angular θ and radial r dependence [16]. They resemble pretty much the solutions found in Subsection III E 1 for the hollow cylinder.

3. TE modes

TE modes satisfy $E_z = 0$ and $B_z \neq 0$. The boundary condition writes this time, for $n \geq 0$:

$$J'_n(k_c a) Y'_n(k_c b) - J'_n(k_c b) Y'_n(k_c a) = 0, \quad (22)$$

with again $k^2 = k_c^2 + \beta^2$. The cutoff frequency $\omega_c = c k_c$ is obtained through the zeroes of Eq. (22), which solutions k_c are indexed through $m > 0$. As for TM waves, the coaxial case requires two indexes while the parallel plate needed only one [1]. But there is a subtlety when $n = 0$; we therefore give first the transverse profiles in Tab. III for $n > 0$, and treat then in Tab. IV the $n = 0$ case separately.

TABLE III. Dimensionless modal profiles for $\text{TE}_{n,m}$ modes in a coaxial waveguide ($n > 0, m > 0$). We defined $A_{n,m} = -\frac{2k_n}{k_c^2 a} \frac{J_n(k_c a) [Y_{n-1}(k_c a) - Y_{n+1}(k_c a)] - [J_{n-1}(k_c a) - J_{n+1}(k_c a)] Y_n(k_c a)}{[Y_{n-1}(k_c a) - Y_{n+1}(k_c a)]}$.

Function	Expression
$g_{E_r}(r, \theta)$	$= -\frac{2k_n}{k_c^2 r A_{n,m}} \left[J_n(k_c r) - \frac{[J_{n-1}(k_c a) - J_{n+1}(k_c a)]}{[Y_{n-1}(k_c a) - Y_{n+1}(k_c a)]} Y_n(k_c r) \right] \sin[n(\theta - \theta_0)]$
$g_{E_\theta}(r, \theta)$	$= -\frac{k}{k_c A_{n,m}} \left(\left[J_{n-1}(k_c r) - J_{n+1}(k_c r) \right] - \frac{[J_{n-1}(k_c a) - J_{n+1}(k_c a)]}{[Y_{n-1}(k_c a) - Y_{n+1}(k_c a)]} [Y_{n-1}(k_c r) - Y_{n+1}(k_c r)] \right) \cos[n(\theta - \theta_0)]$
$g_{E_z}(r, \theta)$	$= 0$
$g_{B_r}(r, \theta)$	$= +\frac{\beta}{k_c A_{n,m}} \left(\left[J_{n-1}(k_c r) - J_{n+1}(k_c r) \right] - \frac{[J_{n-1}(k_c a) - J_{n+1}(k_c a)]}{[Y_{n-1}(k_c a) - Y_{n+1}(k_c a)]} [Y_{n-1}(k_c r) - Y_{n+1}(k_c r)] \right) \cos[n(\theta - \theta_0)]$
$g_{B_\theta}(r, \theta)$	$= -\frac{2\beta n}{k_c^2 r A_{n,m}} \left[J_n(k_c r) - \frac{[J_{n-1}(k_c a) - J_{n+1}(k_c a)]}{[Y_{n-1}(k_c a) - Y_{n+1}(k_c a)]} Y_n(k_c r) \right] \sin[n(\theta - \theta_0)]$
$g_{B_z}(r, \theta)$	$= -\frac{2}{A_{n,m}} \left[J_n(k_c r) - \frac{[J_{n-1}(k_c a) - J_{n+1}(k_c a)]}{[Y_{n-1}(k_c a) - Y_{n+1}(k_c a)]} Y_n(k_c r) \right] \cos[n(\theta - \theta_0)]$

E and **B** fields display again an angular θ and radial r dependence [16]. These modes resemble the ones present in a hollow cylinder, see Section III E 2. For $n > 0$, the normalization has been chosen according to the electric field convention discussed in Section III C. However, for $n = 0$ *the electric field is zero on the conductors*: this brings us to the concept of *virtual electrodes* introduced in Ref. [1]. Looking at Tab. IV, one realizes that the metallic boundary conditions Eqs. (9-12) are met by all planes cutting the coaxial guide as a diameter, see Fig. 1. Within any of these equivalent planes, one can then define *virtual charges and virtual currents* (see Section IV). Following the same philosophy as for real electrodes, we chose to normalize the electric field to its maximal amplitude, namely $|g_{E_\theta}(r = r_{max})| = 1$. r_{max} is defined as the solution of:

$$\frac{J_0(k_c r) - J_2(k_c r)}{Y_0(k_c r) - Y_2(k_c r)} - \frac{J_1(k_c a)}{Y_1(k_c a)} = 0, \quad (23)$$

which is the closest to $r = a$. The normalization amplitude A_m is then computed numerically.

In all the preceding results, they are some differences, but more interestingly strong similarities with the Cartesian case [1]. We will discuss this explicitly in the following Subsection.

TABLE IV. Dimensionless modal profiles for $\text{TE}_{n=0,m}$ modes in a coaxial waveguide ($m > 0$). See text for definition of $A_{n=0,m} = +A_m \frac{k a}{[Y_{-1}(k_c a) - Y_{+1}(k_c a)]}$.

Function	Expression
$g_{E_r}(r, \theta)$	$= 0$
$g_{E_\theta}(r, \theta)$	$= -\frac{k}{k_c A_{0,m}} \left(\left[J_{-1}(k_c r) - J_{+1}(k_c r) \right] - \frac{[J_{-1}(k_c a) - J_{+1}(k_c a)]}{[Y_{-1}(k_c a) - Y_{+1}(k_c a)]} [Y_{-1}(k_c r) - Y_{+1}(k_c r)] \right)$
$g_{E_z}(r, \theta)$	$= 0$
$g_{B_r}(r, \theta)$	$= +\frac{\beta}{k_c A_{0,m}} \left(\left[J_{-1}(k_c r) - J_{+1}(k_c r) \right] - \frac{[J_{-1}(k_c a) - J_{+1}(k_c a)]}{[Y_{-1}(k_c a) - Y_{+1}(k_c a)]} [Y_{-1}(k_c r) - Y_{+1}(k_c r)] \right)$
$g_{B_\theta}(r, \theta)$	$= 0$
$g_{B_z}(r, \theta)$	$= -\frac{2}{A_{0,m}} \left[J_0(k_c r) - \frac{[J_{-1}(k_c a) - J_{+1}(k_c a)]}{[Y_{-1}(k_c a) - Y_{+1}(k_c a)]} Y_0(k_c r) \right]$

4. Comparison with Cartesian geometry

Let us define $b = a + d$ with $d \ll a$, and $w = 2\pi a$. d is thus the gap between electrodes, and w their transverse dimension (perimeter). Consider first the TEM wave: in Tab. I, one obtains $g_{E_r} \approx 1$ and $g_{B_\theta} \approx \text{sign}(\beta)$, which reproduce the Cartesian components of Ref. [1]. Besides, Eqs. (21,22) lead then to the simple solution:

$$k_c = m \frac{\pi}{d}, \quad m \in \mathbb{N}^*, \quad (24)$$

for any n . For $n = 0$, the TM and TE solutions reproduce what is found in Ref. [1]. The interpretation of these modes becomes then clear: they correspond to the parallel plate guide *closed on itself*, with a large enough radius of curvature $\rho \gg a$. The *virtual electrodes* of the TE parallel plate configuration, which are at the boundaries of the guide, transform naturally into the diameter planes discussed in the present manuscript (see Fig. 1).

But what about $n \neq 0$ solutions? These are actually reminiscent of the hollow cylinder configuration discussed in the following: these can be obtained by taking $a/b \rightarrow 0$, and modifying the normalization of the modal functions for $A_{n,m}$ (taking this time the outer guide as a reference). These modes cannot exist between the parallel plates because the symmetry imposes a strict translation invariance (compatible only with the $n = 0$ solution of this Section), while the coaxial line provides periodic boundary conditions ($x \rightarrow x + m w$ for x the transverse component, corresponding to the \mathbf{u}_θ direction here, $m \in \mathbb{N}^*$).

The parallel plate configuration can also be continuously transformed into another type of guide, by rolling up each electrode on itself (creating a cylindrical bar). In the opposite limit where $d \gg a$, one obtains what is called a *bifilar waveguide* [16]. In this open geometry, only TEM modes are allowed.

E. Hollow cylindrical waveguide

In a single wall cylindrical waveguide, no TEM mode exists [16]; the hollow guide supports only TM ($E_z \neq 0$ and $B_z = 0$) and TE ($B_z \neq 0$ and $E_z = 0$) families, which will be described below.

1. TM modes

Regularity at $r = 0$ removes the Bessel Y_n contribution, Eq. (2). The boundary condition $E_z(r = a, \theta) = 0$ leads to:

$$J_n(k_c a) = 0, \quad (25)$$

with similarly to the coaxial line $k^2 = k_c^2 + \beta^2$ and $\omega_c = c k_c$. For each $n \geq 0$, the solutions to the above equation are indexed by $m > 0$. Modal profiles (properly normalized) are summarized in Tab. V.

TABLE V. Dimensionless modal profiles for $\text{TM}_{m,n}$ in a hollow cylindrical waveguide ($n \geq 0, m > 0$). We defined $A_{n,m} = +\frac{\beta}{k_c} [J_{n-1}(k_c a) - J_{n+1}(k_c a)]$.

Function	Expression
$g_{E_r}(r, \theta)$	$= -\frac{\beta}{k_c A_{n,m}} [J_{n-1}(k_c r) - J_{n+1}(k_c r)] \cos[n(\theta - \theta_0)]$
$g_{E_\theta}(r, \theta)$	$= +\frac{2\beta n}{k_c^2 r A_{n,m}} J_n(k_c r) \sin[n(\theta - \theta_0)]$
$g_{E_z}(r, \theta)$	$= +\frac{2}{A_{n,m}} J_n(k_c r) \cos[n(\theta - \theta_0)]$
$g_{B_r}(r, \theta)$	$= -\frac{2k n}{k_c^2 r A_{n,m}} J_n(k_c r) \sin[n(\theta - \theta_0)]$
$g_{B_\theta}(r, \theta)$	$= -\frac{k}{k_c A_{n,m}} [J_{n-1}(k_c r) - J_{n+1}(k_c r)] \cos[n(\theta - \theta_0)]$
$g_{B_z}(r, \theta)$	$= 0$

These modes share the same properties as their Cartesian counterpart. Note however that the index $n = 0$ was excluded in this case [1]: even the lowest TM solutions have an oscillation pattern on *both axes* \mathbf{x}, \mathbf{y} . Here, the $n = 0$ modes oscillate along \mathbf{u}_r , but not along \mathbf{u}_θ . This is a peculiarity arising again from the higher symmetry of the cylindrical geometry.

TABLE VI. Dimensionless modal profiles for $\text{TE}_{m,n}$ in a hollow cylindrical waveguide ($n > 0, m > 0$). We defined $A_{n,m} = +\frac{2k n}{k_c^2 a} J_n(k_c a)$.

Function	Expression
$g_{E_r}(r, \theta)$	$= -\frac{2k n}{k_c^2 r A_{n,m}} J_n(k_c r) \sin[n(\theta - \theta_0)]$
$g_{E_\theta}(r, \theta)$	$= -\frac{k}{k_c A_{n,m}} [J_{n-1}(k_c r) - J_{n+1}(k_c r)] \cos[n(\theta - \theta_0)]$
$g_{E_z}(r, \theta)$	$= 0$
$g_{B_r}(r, \theta)$	$= +\frac{\beta}{k_c A_{n,m}} [J_{n-1}(k_c r) - J_{n+1}(k_c r)] \cos[n(\theta - \theta_0)]$
$g_{B_\theta}(r, \theta)$	$= -\frac{2\beta n}{k_c^2 r A_{n,m}} J_n(k_c r) \sin[n(\theta - \theta_0)]$
$g_{B_z}(r, \theta)$	$= -\frac{2}{A_{n,m}} J_n(k_c r) \cos[n(\theta - \theta_0)]$

2. TE modes

Again regularity at $r = 0$ imposes the absence of Y_n in the solution Eq. (2). The boundary condition $E_\theta(r = a, \theta) = 0$ gives $J'_n(k_c a) = 0$, namely:

$$J_{n-1}(k_c a) = J_{n+1}(k_c a), \quad (26)$$

with as previously $k^2 = k_c^2 + \beta^2$ and $\omega_c = c k_c$. The k_c that solve the above equation are indexed by $m > 0$, for $n \geq 0$.

As for the coaxial line, we should distinguish the $n \neq 0$ from the $n = 0$ cases. Modal profiles for $n > 0$ are summarized in Tab. VI. The normalization discussed in Section III C has been applied. The $n = 0$ modes are presented in Tab. VII. Their understanding requires the introduction of *virtual electrodes*, as discussed in Subsection III D 3.

TABLE VII. Dimensionless modal profiles for $\text{TE}_{n=0,m}$ in a hollow cylindrical waveguide ($m > 0$).

See text for $A_{n=0,m} = +A_m k/k_c$.

Function	Expression
$g_{E_r}(r)$	$= 0$
$g_{E_\theta}(r)$	$= -\frac{k}{k_c A_{0,m}} [J_{-1}(k_c r) - J_{+1}(k_c r)]$
$g_{E_z}(r)$	$= 0$
$g_{B_r}(r)$	$= +\frac{\beta}{k_c A_{0,m}} [J_{-1}(k_c r) - J_{+1}(k_c r)]$
$g_{B_\theta}(r)$	$= 0$
$g_{B_z}(r)$	$= -\frac{2}{A_{0,m}} J_0(k_c r)$

Inspecting Tab. VII, we see that similarly to the $\text{TE}_{0,m}$ modes of the coaxial line, the planes cutting the hollow guide through a diameter verify metallic boundary conditions (see Fig. 1). These will enable to define the *virtual charges and currents* in the following. The required normalization condition reads again $|g_{E_\theta}(r = r_{max})| = 1$, with this time r_{max} solution of:

$$J_0(k_c r) - J_2(k_c r) = 0, \quad (27)$$

which is the closest to $r = 0$. The A_m parameter is then computed numerically. Note that these modes are *different* from their Cartesian counterpart [1]: in a square guide, both $\text{TE}_{0,m}$

and $\text{TE}_{n,0}$ are allowed, and simply correspond to equivalent patterns, rotated by 90° around the \mathbf{z} axis. Here, we have only one family $\text{TE}_{0,m}$ with $m > 0$. Besides, for the square guide the boundary conditions apply directly to the real electrodes, either the top/bottom pair or the left/right: *there is no virtual electrode*. The $\text{TE}_{0,m}$ modes of the cylinder are in this sense quite peculiar, and do not have an equivalent in the Cartesian geometry, again because of their higher symmetry. This specificity will be further discussed in Subsection V C.

IV. CHARGES, CURRENTS, AND CONSTANTS OF MOTION IN CYLINDRICAL GEOMETRY

Surface charge densities σ_s and surface currents \mathbf{j}_s , as defined by the conditions Eqs. (9-12), when combined with Eq. (8) verify charge conservation:

$$\text{div}_s \mathbf{j}_s + \frac{\partial \sigma_s}{\partial t} = 0, \quad (28)$$

with div_s the divergence operator calculated on the s surface. This surface can be part of a curved cylinder (real electrodes with *in,out* or *front,back* subscripts), or a flat diameter plane (virtual ones, with a *vir top,vir bottom* subscript), see Fig. 1.

A. Constants of motion of the electromagnetic field

Following Ref. [1], the constants of motion are obtained by volume integration:

$$H = \int_0^L \int_{r_{\min}}^{r_{\max}} \int_0^{2\pi} \left[\frac{\epsilon}{2} \mathbf{E}(\mathbf{r}, t)^2 + \frac{1}{2\mu} \mathbf{B}(\mathbf{r}, t)^2 \right] r d\theta dr dz, \quad (\text{energy}). \quad (29)$$

$$\mathbf{P} = \int_0^L \int_{r_{\min}}^{r_{\max}} \int_0^{2\pi} \epsilon [\mathbf{E}(\mathbf{r}, t) \times \mathbf{B}(\mathbf{r}, t)] r d\theta dr dz, \quad (\text{momentum}), \quad (30)$$

$$\mathbf{J} = \int_0^L \int_{r_{\min}}^{r_{\max}} \int_0^{2\pi} \mathbf{r} \times \left\{ \epsilon [\mathbf{E}(\mathbf{r}, t) \times \mathbf{B}(\mathbf{r}, t)] \right\} r d\theta dr dz, \quad (\text{angular momentum}). \quad (31)$$

For the coaxial line, $r_{\min} = a$ and $r_{\max} = b$ while for the hollow cylinder we have $r_{\min} = 0$, $r_{\max} = a$. By symmetry about the guide axis, in \mathbf{P} only the longitudinal momentum P_z is nonzero; \mathbf{J} is always identically zero. Consequently, just as in the Cartesian analysis, the field configurations are fully characterized by the pair $\{H, P_z\}$ (energy and longitudinal momentum). Thus, the light helicity does not play any role here.

B. Generalized fluxes

At this stage, we must introduce surface capacitance densities (in F/m^2) and "inverse inductance densities" (actually, in H^{-1} , see Section VI), which are defined for each electrode type. They are obtained from a specific lengthscale h_{eff} which depends on the geometry, and will be given below for each specific case. Explicitly, we write:

$$C_d = \frac{\epsilon}{h_{\text{eff}}}, \quad (32)$$

$$L_d^{-1} = \frac{1}{\mu h_{\text{eff}}}. \quad (33)$$

Let us point out two subtle differences with the Cartesian configuration. On one hand, the cylindrical geometry is more symmetric: the surfaces facing each other are of one kind only, while in a rectangular guide with width w different from height d ($w \neq d$) *two sets* of electrodes must be considered [1]. However, on the other hand in the parallel plate guide, the two electrodes confining the field are strictly identical, while in a coaxial line one is smaller than the other: *they are not equivalent*. In this case, we will use a prime to designate quantities corresponding to the electrode opposite to the reference one.

On the same model as what is performed in Ref. [1], these lengthscales enable to define *generalized fluxes* with a magnitude given by:

$$\phi_m = \frac{E_m h_{\text{eff}}}{\omega}. \quad (34)$$

These generalized fluxes live on the electrodes. When they correspond to real ones (the metallic guides), we have:

$$\varphi(\theta, z, t) = \phi_m g_{\text{real}}(\theta) \tilde{f}(z, t), \quad (35)$$

while when electrodes are virtual (diameter planes, Fig. 1) we write:

$$\varphi(r, z, t) = \phi_m g_{\text{vir}}(r) \tilde{f}(z, t). \quad (36)$$

The $g_{\text{real}}, g_{\text{vir}}$ functions represent the variations of the fluxes over the electrodes. The point will be in the following to re-express the constants of motion as a function of these φ quantities. We shall then introduce the canonically-conjugate variable Q , enabling the quantization of the φ, Q pair. A proper gauge fixing must then link φ to the electromagnetic potentials \mathbf{A}, V . We demonstrate that the formalism developed for the Cartesian geometry [1] can be adapted to the specificities of the cylindrical symmetry.

C. Coaxial waveguide

1. TEM modes

As for the Cartesian case, the simplest wave propagation concerns TEM modes. We define:

$$h_{\text{eff}} = a \ln \left[\frac{b}{a} \right], \quad (37)$$

$$h'_{\text{eff}} = \frac{b}{a} h_{\text{eff}}, \quad (38)$$

$$\text{and:} \quad (39)$$

$$g_{\text{real}}(\theta) = 1. \quad (40)$$

The boundary conditions on the inner electrode bring:

$$\sigma_{in} = +C_d \frac{\partial \varphi(\theta, z, t)}{\partial t}, \quad (41)$$

$$\mathbf{j}_{in} = -L_d^{-1} \frac{\partial \varphi(\theta, z, t)}{\partial z} \mathbf{z}, \quad (42)$$

while on the outer one we have:

$$\sigma_{out} = -C'_d \frac{\partial \varphi(\theta, z, t)}{\partial t}, \quad (43)$$

$$\mathbf{j}_{out} = +L_d'^{-1} \frac{\partial \varphi(\theta, z, t)}{\partial z} \mathbf{z}, \quad (44)$$

with reversed signs. Note that it is the same φ function (calculated with h_{eff}) that appears in the above; only the capacitance and inductance densities are different from the reference ones (and are calculated with h'_{eff}). Energy and momentum write:

$$H = \int_0^L \int_0^{2\pi} \left[\frac{1}{2} C_d \left(\frac{\partial \varphi(\theta, z, t)}{\partial t} \right)^2 + \frac{1}{2} L_d^{-1} \left(\frac{\partial \varphi(\theta, z, t)}{\partial z} \right)^2 \right] a d\theta dz, \quad (45)$$

$$\mathbf{P} = \int_0^L \int_0^{2\pi} C_d \left[-\frac{\partial \varphi(\theta, z, t)}{\partial t} \frac{\partial \varphi(\theta, z, t)}{\partial z} \right] a d\theta dz \mathbf{z}, \quad (46)$$

and the charge conservation equation Eq. (28) leads to:

$$\frac{\partial^2 \varphi(\theta, z, t)}{\partial z^2} - \frac{1}{c^2} \frac{\partial^2 \varphi(\theta, z, t)}{\partial t^2} = 0, \quad (47)$$

which is nothing but the conventional (d'Alembert) wave propagation equation for φ , at the speed of light c in the medium. Finally, the bracket in Eq. (45) can be identified with the

surface charge/current energy density H_d :

$$H_d = \frac{1}{2} C_d^{-1} \sigma_{in}^2 + \frac{1}{2} L_d \mathbf{j}_{in}^2. \quad (48)$$

Note - Obviously, a completely similar writing can be achieved while referencing the fields on the outer electrode, defining properly alternative h_{eff} and h'_{eff} quantities; the integrations run then onto an arc $b d\theta$ instead of $a d\theta$. This is also true for any of the other configurations considered below dealing with real electrodes.

2. TM modes

For TM modes, we define:

$$h_{\text{eff}} = a \frac{\pi^2}{2} \int_a^b \frac{k_c^2 r}{2} (J_n[k_c r] Y_n[k_c a] - J_n[k_c a] Y_n[k_c r])^2 dr, \quad (49)$$

$$h'_{\text{eff}} = \frac{b}{a} \left| \frac{J_n(k_c b)}{J_n(k_c a)} \right| h_{\text{eff}}, \quad (50)$$

$$\text{and:} \quad (51)$$

$$g_{\text{real}}(\theta) = \cos[n(\theta - \theta_0)], \quad (52)$$

This time, the expression of h_{eff} is not analytic, and must be computed numerically. The metallic boundary condition on the inner electrode writes here:

$$\sigma_{in} = +C_d \frac{\partial \varphi(\theta, z, t)}{\partial t}, \quad (53)$$

$$\mathbf{j}_{in} = -L_d^{-1} \left(\frac{k}{\beta} \right)^2 \frac{\partial \varphi(\theta, z, t)}{\partial z} \mathbf{z}, \quad (54)$$

and on the outer one we obtain:

$$\sigma_{out} = -(-1)^m C_d' \frac{\partial \varphi(\theta, z, t)}{\partial t}, \quad (55)$$

$$\mathbf{j}_{out} = +(-1)^m L_d'^{-1} \left(\frac{k}{\beta} \right)^2 \frac{\partial \varphi(\theta, z, t)}{\partial z} \mathbf{z}. \quad (56)$$

As for TEM modes, the primed quantities are computed from h'_{eff} ; the $(-1)^m$ sign factor arises from the sign of $J_n(k_c b)/J_n(k_c a)$, characteristic of the symmetry of the mode profile.

Energy and momentum are obtained as:

$$H = \int_0^L \int_0^{2\pi} \left[\frac{1}{2} C_d \left(\frac{\partial \varphi(\theta, z, t)}{\partial t} \right)^2 + \frac{1}{2} C_d \left(\frac{k}{\beta} \right)^2 (c k_c)^2 \varphi(\theta, z, t)^2 + \frac{1}{2} L_d^{-1} \left(\frac{k}{\beta} \right)^4 \left(\frac{\partial \varphi(\theta, z, t)}{\partial z} \right)^2 \right] a d\theta dz, \quad (57)$$

$$\mathbf{P} = \int_0^L \int_0^{2\pi} C_d \left(\frac{k}{\beta} \right)^2 \left[-\frac{\partial \varphi(\theta, z, t)}{\partial t} \frac{\partial \varphi(\theta, z, t)}{\partial z} \right] a d\theta dz \mathbf{z}. \quad (58)$$

The propagation equation derived from charge conservation is then:

$$\frac{\partial^2 \varphi(\theta, z, t)}{\partial z^2} - \frac{1}{v_\phi^2} \frac{\partial^2 \varphi(\theta, z, t)}{\partial t^2} = 0, \quad (59)$$

where $v_\phi = c k / |\beta|$. The bracket in Eq. (57) can be understood as the integral over a surface energy density H_d :

$$H_d = \frac{1}{2} C_d^{-1} \sigma_{in}^2 + \frac{1}{2} L_d \mathbf{j}_{in}^2 + \Delta(\theta, z, t), \quad (60)$$

but this time with an addendum term Δ :

$$\Delta(\theta, z, t) = \frac{1}{2} C_d \left(\frac{k}{\beta} \right)^2 (c k_c)^2 \varphi(\theta, z, t)^2, \quad (61)$$

which can be interpreted (as in the Cartesian case) as the *potential energy cost* required to confine a TM wave.

3. TE modes

Finally, the last situation to describe is TE modes. Let us consider first $n > 0$. In this case, we define:

$$h_{\text{eff}} = a \frac{2}{n^2} \int_a^b \frac{k_c^2 r}{2} \left(\frac{(J_{n+1}[k_c a] - J_{n-1}[k_c a]) Y_n[k_c r] - J_n[k_c r] (Y_{n+1}[k_c a] - Y_{n-1}[k_c a])}{(J_{n+1}[k_c a] - J_{n-1}[k_c a]) Y_n[k_c a] - J_n[k_c a] (Y_{n+1}[k_c a] - Y_{n-1}[k_c a])} \right)^2 dr, \quad (62)$$

$$h'_{\text{eff}} = \frac{b}{a} \left| \frac{\pi}{4} (k_c b) [(J_{n+1}[k_c b] - J_{n-1}[k_c b]) Y_n[k_c a] - J_n[k_c a] (Y_{n+1}[k_c b] - Y_{n-1}[k_c b])] \right| h_{\text{eff}}, \quad (63)$$

$$\text{and:} \quad (64)$$

$$g_{\text{real}}(\theta) = \sin[n(\theta - \theta_0)]. \quad (65)$$

As for TM modes, h_{eff} must be computed numerically. From the boundary conditions of Section III B, we obtain:

$$\sigma_{in} = +C_d \frac{\partial \varphi(\theta, z, t)}{\partial t}, \quad (66)$$

$$\mathbf{j}_{in} = -L_d^{-1} \frac{\partial \varphi(\theta, z, t)}{\partial z} \mathbf{z} - L_d^{-1} \left(\frac{k_c^2 a^2}{n^2} \right) \frac{1}{a} \frac{\partial \varphi(\theta, z, t)}{\partial \theta} \mathbf{u}_\theta. \quad (67)$$

A new term appeared in Eq. (67): a peripheral current flows in the electrode, due to the longitudinal magnetic field component. Similarly, on the other electrode we have:

$$\sigma_{out} = -(-1)^{m+1} C'_d \frac{\partial \varphi(\theta, z, t)}{\partial t}, \quad (68)$$

$$\mathbf{j}_{out} = +(-1)^{m+1} L_d'^{-1} \frac{\partial \varphi(\theta, z, t)}{\partial z} \mathbf{z} + (-1)^{m+1} L_d'^{-1} \left(\frac{k_c^2 b^2}{n^2} \right) \frac{1}{b} \frac{\partial \varphi(\theta, z, t)}{\partial \theta} \mathbf{u}_\theta, \quad (69)$$

with primed quantities defined with h'_{eff} . The sign change $(-1)^{m+1}$ is due to the sign of the expression within the absolute value bars in Eq. (63). At first sight, this $m+1$ (symmetry related) exponent seems different from the one found in Ref. [1]; but it is actually a trivial consequence of the numbering. These TE $n \neq 0$ modes are reminiscent of the hollow cylinder configuration, which correspond for Cartesian geometries to the rectangular guide. Their numbering starts at $m=0$ when $n>0$, while here it starts at $m=1$. The expressions for energy and momentum are:

$$H = \int_0^L \int_0^{2\pi} \left[\frac{1}{2} C_d \left(\frac{\partial \varphi(\theta, z, t)}{\partial t} \right)^2 + \frac{1}{2} L_d^{-1} \left(\frac{\partial \varphi(\theta, z, t)}{\partial z} \right)^2 + \frac{1}{2} L_d^{-1} \frac{k_c^2 a^2}{n^2} \left(\frac{1}{a} \frac{\partial \varphi(\theta, z, t)}{\partial \theta} \right)^2 \right] a d\theta dz, \quad (70)$$

$$\mathbf{P} = \int_0^L \int_0^{2\pi} C_d \left[-\frac{\partial \varphi(\theta, z, t)}{\partial t} \frac{\partial \varphi(\theta, z, t)}{\partial z} \right] a d\theta dz \mathbf{z}. \quad (71)$$

The charge conservation equation brings us this time:

$$\frac{\partial^2 \varphi(\theta, z, t)}{\partial z^2} - \frac{1}{c^2} \frac{\partial^2 \varphi(\theta, z, t)}{\partial t^2} = k_c^2 \varphi(\theta, z, t), \quad (72)$$

which is a *Klein-Gordon* propagation equation. Here, the term $\hbar k_c/c$ plays the role of a mass: there is a kinetic energy cost when confining TE waves (while there is a potential one for TM). This will be discussed in more details in Section VI. Once again, the bracket in Eq. (70) can be recast into a surface energy density H_d :

$$H_d = \frac{1}{2} C_d^{-1} \sigma_{in}^2 + \frac{1}{2} L_d (\mathbf{j}_{in} \cdot \mathbf{z})^2 + \frac{1}{2} L_d \frac{n^2}{k_c^2 a^2} (\mathbf{j}_{in} \cdot \mathbf{u}_\theta)^2. \quad (73)$$

The peripheral currents, to which we associate an inductance density $L_d \frac{n^2}{k_c^2 a^2}$, are therefore associated to the mass appearance.

Consider now the $n=0$ situation. The peculiarity there is that the transverse fields are zero on the metallic guides, see Subsection III D 3. We must thus introduce the concept of

virtual electrodes, with:

$$h_{\text{eff}} = a \int_a^b \frac{4r}{a^2} \left(\frac{J_1[k_c r] Y_1[k_c a] - J_1[k_c a] Y_1[k_c r]}{A_m(k_c a)} \right)^2 dr, \quad (74)$$

$$\text{and:} \quad (75)$$

$$g_{vir}(r) = 2 \left(\frac{J_1[k_c a] Y_1[k_c r] - J_1[k_c r] Y_1[k_c a]}{A_m(k_c a)} \right), \quad (76)$$

and A_m obtained numerically (Subsection III D 3). h_{eff} is again non-analytic. Any diameter plane crossing the coaxial line can be taken as virtual electrode. Charges and currents are defined there as:

$$\sigma_{vir\ top} = +C_d \frac{\partial \varphi(r, z, t)}{\partial t}, \quad (77)$$

$$\mathbf{j}_{vir\ top} = -L_d^{-1} \frac{\partial \varphi(r, z, t)}{\partial z} \mathbf{z} - L_d^{-1} \frac{1}{r} \frac{\partial (r \varphi[r, z, t])}{\partial r} \mathbf{u}_r, \quad (78)$$

for the top part of the plane, for which we took $+\mathbf{u}_\theta$ as normal (see Fig. 1). The bottom part is oriented the other way, leading to:

$$\sigma_{vir\ bottom} = -C_d \frac{\partial \varphi(r, z, t)}{\partial t}, \quad (79)$$

$$\mathbf{j}_{vir\ bottom} = +L_d^{-1} \frac{\partial \varphi(r, z, t)}{\partial z} \mathbf{z} + L_d^{-1} \frac{1}{r} \frac{\partial (r \varphi[r, z, t])}{\partial r} \mathbf{u}_r. \quad (80)$$

On each real conductor, a peripheral current is flowing:

$$\mathbf{j}_{in} = +L_d^{-1} 2k_c \left(\frac{J_1[k_c a] Y_0[k_c a] - J_0[k_c a] Y_1[k_c a]}{A_m(k_c a)} \right) \phi_m \tilde{f}(z, t) \mathbf{u}_\theta, \quad (81)$$

$$\mathbf{j}_{out} = -L_d^{-1} 2k_c \left(\frac{J_1[k_c a] Y_0[k_c b] - J_0[k_c b] Y_1[k_c a]}{A_m(k_c a)} \right) \phi_m \tilde{f}(z, t) \mathbf{u}_\theta. \quad (82)$$

These can be seen as connected by continuity in $r = a$ and $r = b$ by the virtual current component flowing in the direction $\pm \mathbf{u}_r$; this is depicted in Fig. 2. Energy and momentum are then deduced with:

$$H = \int_0^L \int_a^b \left[\frac{1}{2} C_d \left(\frac{\partial \varphi(r, z, t)}{\partial t} \right)^2 + \frac{1}{2} L_d^{-1} \left(\frac{\partial \varphi(r, z, t)}{\partial z} \right)^2 + \frac{1}{2} L_d^{-1} \left(\frac{1}{r} \frac{\partial (r \varphi[r, z, t])}{\partial r} \right)^2 \right] \frac{2\pi r}{h_{\text{eff}}} dr dz, \quad (83)$$

$$\mathbf{P} = \int_0^L \int_a^b C_d \left[-\frac{\partial \varphi(r, z, t)}{\partial t} \frac{\partial \varphi(r, z, t)}{\partial z} \right] \frac{2\pi r}{h_{\text{eff}}} dr dz \mathbf{z}. \quad (84)$$

The specific writing of these expressions will be commented below. Charge conservation is applied in the virtual plane, treating z, r as coordinates of a flat surface. One obtains:

$$\frac{\partial^2 \varphi(r, z, t)}{\partial z^2} - \frac{1}{c^2} \frac{\partial^2 \varphi(r, z, t)}{\partial t^2} = k_c^2 \varphi(r, z, t), \quad (85)$$

which reads essentially the same as Eq. (72). There is indeed a geometrical subtlety here, arising from the mapping of the curved problem onto a plane, which leads to the normalization by h_{eff} in the H and \mathbf{P} expressions. The bracket in Eq. (83) can still be interpreted as a charge/current energy density H_d , but with properly defined (and r -dependent) capacitance and inductance densities:

$$H_d = \frac{1}{2} \left[C_d^{-1} \frac{2\pi r}{h_{\text{eff}}} \right] \sigma_{vir\ top}^2 + \frac{1}{2} \left[L_d \frac{2\pi r}{h_{\text{eff}}} \right] (\mathbf{j}_{vir\ top} \cdot \mathbf{z})^2 + \frac{1}{2} \left[L_d \frac{2\pi r}{h_{\text{eff}}} \right] (\mathbf{j}_{vir\ top} \cdot \mathbf{u}_r)^2, \quad (86)$$

written in brackets in this formula. The same expression holds obviously for the *vir bottom* terms. As for the $n > 0$ case, the light confinement in the guide comes with a kinetic cost, due to the peripheral currents.

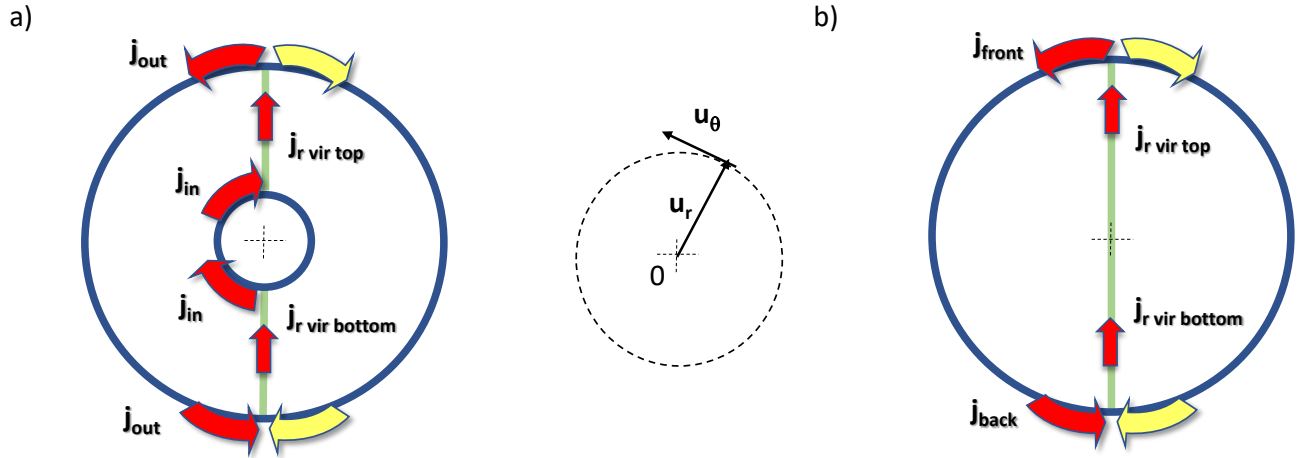


FIG. 2. Transverse currents of TE modes with $n = 0$. a) coaxial case. b) hollow cylinder. The direction of the outer current circulation depends on the mode number m ; for the coaxial line, it is also a function of the ratio b/a (but the behavior becomes equivalent to the hollow guide at $b/a \gg 1$). Considering this limit, we represent in red the m even case; the outer current is reversed for m odd (yellow).

D. Hollow cylindrical waveguide

1. TM modes

The TM modes of the hollow guide lead to:

$$h_{\text{eff}} = a \left[2 \left(\frac{J_{n-1}[k_c a]}{J_{n-1}[k_c a] - J_{n+1}[k_c a]} \right)^2 \right], \quad (87)$$

and:

$$g_{\text{real}}(\theta) = \cos[n(\theta - \theta_0)]. \quad (89)$$

Charges and currents on the cylinder read:

$$\sigma_{\text{front}} = +C_d \frac{\partial \varphi(\theta, z, t)}{\partial t}, \quad (90)$$

$$\mathbf{j}_{\text{front}} = -L_d^{-1} \left(\frac{k}{\beta} \right)^2 \frac{\partial \varphi(\theta, z, t)}{\partial z} \mathbf{z}, \quad (91)$$

on the "front" side, and we obtain on the "back" side $\theta \rightarrow \theta + \pi$:

$$\sigma_{\text{back}} = -(-1)^{n+1} C_d \frac{\partial \varphi(\theta, z, t)}{\partial t}, \quad (92)$$

$$\mathbf{j}_{\text{back}} = +(-1)^{n+1} L_d^{-1} \left(\frac{k}{\beta} \right)^2 \frac{\partial \varphi(\theta, z, t)}{\partial z} \mathbf{z}. \quad (93)$$

This $(-1)^{n+1}$ sign change (due to the mode symmetry) seems in the first place different from what is found in Ref. [1]. But it is a trivial consequence of the basis vector \mathbf{u}_r being always oriented towards the outside of the guide. Energy and momentum write:

$$H = \int_0^L \int_0^{2\pi} \left[\frac{1}{2} C_d \left(\frac{\partial \varphi(\theta, z, t)}{\partial t} \right)^2 + \frac{1}{2} C_d \left(\frac{k}{\beta} \right)^2 (c k_c)^2 \varphi(\theta, z, t)^2 + \frac{1}{2} L_d^{-1} \left(\frac{k}{\beta} \right)^4 \left(\frac{\partial \varphi(\theta, z, t)}{\partial z} \right)^2 \right] a d\theta dz, \quad (94)$$

$$\mathbf{P} = \int_0^L \int_0^{2\pi} C_d \left(\frac{k}{\beta} \right)^2 \left[-\frac{\partial \varphi(\theta, z, t)}{\partial t} \frac{\partial \varphi(\theta, z, t)}{\partial z} \right] a d\theta dz \mathbf{z}, \quad (95)$$

which are perfectly similar to the ones of the coaxial line (but with the integral $a d\theta$ running on the confining tube). As well, the propagation equation deduced from charge conservation is again:

$$\frac{\partial^2 \varphi(\theta, z, t)}{\partial z^2} - \frac{1}{v_\phi^2} \frac{\partial^2 \varphi(\theta, z, t)}{\partial t^2} = 0, \quad (96)$$

with v_ϕ the phase velocity. The surface integral Eq. (94) can be recast in terms of an energy density:

$$H_d = \frac{1}{2} C_d^{-1} \sigma_{front}^2 + \frac{1}{2} L_d \mathbf{j}_{front}^2 + \Delta(\theta, z, t), \quad (97)$$

following the same logic as for the coaxial line (the same expression can obviously be written with the *back* terms). The addendum term Δ is again:

$$\Delta(\theta, z, t) = \frac{1}{2} C_d \left(\frac{k}{\beta} \right)^2 (c k_c)^2 \varphi(\theta, z, t)^2, \quad (98)$$

and corresponds to a potential energy needed for the confinement of light in the guide.

2. TE modes

Let us present first the $n > 0$ situation. We define:

$$h_{\text{eff}} = a \left(\frac{k_c a}{n} \right)^2 \left(\frac{(k_c a) J_n [k_c a]^2 - 2n J_n [k_c a] J_{n+1} [k_c a] + (k_c a) J_{n+1} [k_c a]^2}{2 (k_c a) J_n [k_c a]^2} \right), \quad (99)$$

and:

$$g_{\text{real}}(\theta) = \sin[n(\theta - \theta_0)]. \quad (101)$$

Charges and currents on the "front" conductor read:

$$\sigma_{front} = +C_d \frac{\partial \varphi(\theta, z, t)}{\partial t}, \quad (102)$$

$$\mathbf{j}_{front} = -L_d^{-1} \frac{\partial \varphi(\theta, z, t)}{\partial z} \mathbf{z} - L_d^{-1} \left(\frac{k_c^2 a^2}{n^2} \right) \frac{1}{a} \frac{\partial \varphi(\theta, z, t)}{\partial \theta} \mathbf{u}_\theta, \quad (103)$$

which reproduces the results found for the coaxial guide. The "back" position being defined by $\theta \rightarrow \theta + \pi$, we obtain:

$$\sigma_{back} = -(-1)^{n+1} C_d \frac{\partial \varphi(\theta, z, t)}{\partial t}, \quad (104)$$

$$\mathbf{j}_{back} = +(-1)^{n+1} L_d^{-1} \frac{\partial \varphi(\theta, z, t)}{\partial z} \mathbf{z} + (-1)^{n+1} L_d^{-1} \left(\frac{k_c^2 a^2}{n^2} \right) \frac{1}{a} \frac{\partial \varphi(\theta, z, t)}{\partial \theta} \mathbf{u}_\theta. \quad (105)$$

The symmetry sign change (which depends here on $n + 1$) seems again different from the one reported in Cartesian geometries [1]. But as for TM waves, this is simply due to the orientation of the basis vector \mathbf{u}_r which always points towards the outside of the guide.

Energy H and momentum \mathbf{P} are written in the same form as for the coaxial guide:

$$H = \int_0^L \int_0^{2\pi} \left[\frac{1}{2} C_d \left(\frac{\partial \varphi(\theta, z, t)}{\partial t} \right)^2 + \frac{1}{2} L_d^{-1} \left(\frac{\partial \varphi(\theta, z, t)}{\partial z} \right)^2 + \frac{1}{2} L_d^{-1} \frac{k_c^2 a^2}{n^2} \left(\frac{1}{a} \frac{\partial \varphi(\theta, z, t)}{\partial \theta} \right)^2 \right] a d\theta dz, \quad (106)$$

$$\mathbf{P} = \int_0^L \int_0^{2\pi} C_d \left[-\frac{\partial \varphi(\theta, z, t)}{\partial t} \frac{\partial \varphi(\theta, z, t)}{\partial z} \right] a d\theta dz \mathbf{z}. \quad (107)$$

The propagation equation deduced from Eq. (28) is also equivalent:

$$\frac{\partial^2 \varphi(\theta, z, t)}{\partial z^2} - \frac{1}{c^2} \frac{\partial^2 \varphi(\theta, z, t)}{\partial t^2} = k_c^2 \varphi(\theta, z, t), \quad (108)$$

displaying the *Klein-Gordon* form specific to TE waves. As well, Eq. (106) corresponds to the surface integral of the density H_d :

$$H_d = \frac{1}{2} C_d^{-1} \sigma_{front}^2 + \frac{1}{2} L_d (\mathbf{j}_{front} \cdot \mathbf{z})^2 + \frac{1}{2} L_d \frac{n^2}{k_c^2 a^2} (\mathbf{j}_{front} \cdot \mathbf{u}_\theta)^2, \quad (109)$$

or equivalently with *back* subscripts. As for the coaxial guide, a mass term $\hbar k_c/c$ appeared, linked directly to the peripheral current.

Let us finally describe TE waves with $n = 0$. As for the coaxial line, virtual electrodes must be used in this case. We define:

$$h_{\text{eff}} = a \left(2 \frac{J_0[k_c a]^2 + J_1[k_c a]^2}{A_m^2} \right), \quad (110)$$

and:

$$g_{vir}(r) = 2 \frac{J_1[k_c r]}{A_m}, \quad (111)$$

and A_m is obtained numerically (Subsection III E 2). Charges and currents on the top part of the virtual plane read:

$$\sigma_{vir top} = +C_d \frac{\partial \varphi(r, z, t)}{\partial t}, \quad (113)$$

$$\mathbf{j}_{vir top} = -L_d^{-1} \frac{\partial \varphi(r, z, t)}{\partial z} \mathbf{z} - L_d^{-1} \frac{1}{r} \frac{\partial (r \varphi[r, z, t])}{\partial r} \mathbf{u}_r, \quad (114)$$

while for the bottom one we have:

$$\sigma_{vir bottom} = -C_d \frac{\partial \varphi(r, z, t)}{\partial t}, \quad (115)$$

$$\mathbf{j}_{vir bottom} = +L_d^{-1} \frac{\partial \varphi(r, z, t)}{\partial z} \mathbf{z} + L_d^{-1} \frac{1}{r} \frac{\partial (r \varphi[r, z, t])}{\partial r} \mathbf{u}_r, \quad (116)$$

the signs are reversed. The peripheral current flowing in the real electrode is:

$$\mathbf{j}_{front} = \mathbf{j}_{back} = -L_d^{-1} 2k_c \left(\frac{J_0[k_c a]}{A_m} \right) \phi_m \tilde{f}(z, t) \mathbf{u}_\theta, \quad (117)$$

which connects to the virtual current by continuity in $r = a$ (see Fig. 2). The constants of motion are then obtained with the integrals:

$$H = \int_0^L \int_0^a \left[\frac{1}{2} C_d \left(\frac{\partial \varphi(r, z, t)}{\partial t} \right)^2 + \frac{1}{2} L_d^{-1} \left(\frac{\partial \varphi(r, z, t)}{\partial z} \right)^2 + \frac{1}{2} L_d^{-1} \left(\frac{1}{r} \frac{\partial (r \varphi[r, z, t])}{\partial r} \right)^2 \right] \frac{2\pi r}{h_{\text{eff}}} dr dz, \quad (118)$$

$$\mathbf{P} = \int_0^L \int_0^a C_d \left[-\frac{\partial \varphi(r, z, t)}{\partial t} \frac{\partial \varphi(r, z, t)}{\partial z} \right] \frac{2\pi r}{h_{\text{eff}}} dr dz \mathbf{z}, \quad (119)$$

exactly like in the coaxial case. We obtain again the Klein-Gordon propagation equation for the generalized flux φ :

$$\frac{\partial^2 \varphi(r, z, t)}{\partial z^2} - \frac{1}{c^2} \frac{\partial^2 \varphi(r, z, t)}{\partial t^2} = k_c^2 \varphi(r, z, t), \quad (120)$$

from the charge conservation equation applied onto the virtual plane. The virtual surface charge/current density is again:

$$H_d = \frac{1}{2} \left[C_d^{-1} \frac{2\pi r}{h_{\text{eff}}} \right] \sigma_{vir\ top}^2 + \frac{1}{2} \left[L_d \frac{2\pi r}{h_{\text{eff}}} \right] (\mathbf{j}_{vir\ top} \cdot \mathbf{z})^2 + \frac{1}{2} \left[L_d \frac{2\pi r}{h_{\text{eff}}} \right] (\mathbf{j}_{vir\ top} \cdot \mathbf{u}_r)^2, \quad (121)$$

and equivalently with a *vir bottom* subscript. The mass term and peripheral current terms, characteristic of a TE wave, appear here exactly like in the coaxial treatment.

V. ELECTROMAGNETIC GAUGE

A keypoint of electromagnetic theory is the existence of scalar and vector potentials V, \mathbf{A} from which Maxwell's physical fields \mathbf{E}, \mathbf{B} can be derived [3]:

$$\mathbf{E}(\mathbf{r}, t) = -\frac{\partial \mathbf{A}(\mathbf{r}, t)}{\partial t} - \nabla V(\mathbf{r}, t), \quad (122)$$

$$\mathbf{B}(\mathbf{r}, t) = \nabla \times \mathbf{A}(\mathbf{r}, t). \quad (123)$$

These potentials are defined up to a transformation:

$$\mathbf{A}(\mathbf{r}, t) \rightarrow \mathbf{A}(\mathbf{r}, t) + \nabla \Pi(\mathbf{r}, t), \quad V(\mathbf{r}, t) \rightarrow V(\mathbf{r}, t) - \frac{\partial \Pi(\mathbf{r}, t)}{\partial t}, \quad (124)$$

with $\Pi(\mathbf{r}, t)$ an arbitrary function called gauge. This fact is known as *gauge invariance*, and is obviously valid for any coordinate system; we shall express it here in the cylindrical geometry.

Following the reasoning of Ref. [1], the relevant gauges should involve our X, Y quadrature variables, and should share the symmetry of the problem at hand. This enables to write:

$$\Pi(\mathbf{r}, t) = p(\mathbf{r}, \theta) f(z, t) + \tilde{p}(\mathbf{r}, \theta) \tilde{f}(z, t), \quad (125)$$

with the potentials verifying the Lorenz gauge condition:

$$\nabla \cdot \mathbf{A}(\mathbf{r}, t) + \frac{1}{c^2} \frac{\partial V(\mathbf{r}, t)}{\partial t} = 0. \quad (126)$$

Any other choice amounts to a trivial invariance with no physical content. Injecting the ansatz Eq. (125) into Eq. (126), we obtain the pair of transverse equations for the gauge profiles:

$$\frac{1}{r} \frac{\partial}{\partial r} \left(r \frac{\partial p(r, \theta)}{\partial r} \right) + \frac{1}{r^2} \frac{\partial^2 p(r, \theta)}{\partial \theta^2} + (k^2 - \beta^2) p(r, \theta) = 0, \quad (127)$$

$$\frac{1}{r} \frac{\partial}{\partial r} \left(r \frac{\partial \tilde{p}(r, \theta)}{\partial r} \right) + \frac{1}{r^2} \frac{\partial^2 \tilde{p}(r, \theta)}{\partial \theta^2} + (k^2 - \beta^2) \tilde{p}(r, \theta) = 0. \quad (128)$$

These equations must be solved for each case, taking into account the proper symmetries. Special care will be required by the TE $n = 0$ modes, which involve virtual electrodes. We shall demonstrate below how a specific gauge choice can then be made, relating \mathbf{A} and V to the generalized flux φ through Devoret-like expressions [2].

TABLE VIII. Gauge description for TEM waves.

Function	Expression
$A_r(r, \theta, z, t)$	$= 0$
$A_\theta(r, \theta, z, t)$	$= 0$
$A_z(r, \theta, z, t)$	$= +\phi_m \beta \left[\frac{1}{2} - \frac{\ln(r/a)}{\ln(b/a)} \right] f(z, t)$
$V(r, \theta, z, t)$	$= +\phi_m \omega \left[\frac{1}{2} - \frac{\ln(r/a)}{\ln(b/a)} \right] f(z, t)$
Gauge fixing	$a_\pi = 0, \tilde{a}_\pi = 0$
Gauge invariance	b_π, \tilde{b}_π

A. Coaxial waveguide

1. TEM modes

For TEM waves, the dispersion relation enforces $k = |\beta|$. Solving Eqs. (127,128) with the azimuthal invariance characteristic of these fields leads to:

$$p(r) = a_\pi \ln r + b_\pi, \quad \tilde{p}(r) = \tilde{a}_\pi \ln r + \tilde{b}_\pi, \quad (129)$$

with $a_\pi, b_\pi, \tilde{a}_\pi, \tilde{b}_\pi$ four real constants. We define here:

$$\Delta V(z, t) = V(r = a, z, t) - V(r = b, z, t), \quad (130)$$

$$\Delta A_z(z, t) = A_z(r = a, z, t) - A_z(r = b, z, t), \quad (131)$$

the potential differences between the electrodes (with no θ dependence). These can be linked to the generalized flux through the relations:

$$\frac{\partial \varphi(\theta, z, t)}{\partial t} = \Delta V(z, t), \quad (132)$$

$$\frac{\partial \varphi(\theta, z, t)}{\partial z} = -\Delta A_z(z, t), \quad (133)$$

which express here the Devoret relationship [1, 2]. Importantly, these formulas are *not gauge invariant* (see Subection V C). The potentials corresponding to this gauge are given in Tab. VIII, written such that $a_\pi, \tilde{a}_\pi = 0$: this is the gauge fixing corresponding to the "Devoret gauge" in the coaxial geometry. We recognize the usual *longitudinal gauge*.

Similarly to the Cartesian case, the b_π, \tilde{b}_π constants are undefined: this is the remaining gauge invariance [1]. Note that the choice made in the tabular is such that potentials have opposite signs on the two electrodes, matching Ref. [1]. This is a pure commodity, and is not required by the modeling, especially since the two electrodes are *different* in size (which breaks the symmetry).

2. TM modes

For TM waves, the dispersion relation reads $k^2 - \beta^2 = k_c^2 > 0$. Eqs. (127,128) therefore lead to the solutions:

$$p(r, \theta) = \left(a_\pi J_n[k_c r] + b_\pi Y_n[k_c r] \right) \cos[n(\theta - \theta_0)] + \left(c_\pi J_n[k_c r] + d_\pi Y_n[k_c r] \right) \sin[n(\theta - \theta_0)], \quad (134)$$

$$\tilde{p}(r, \theta) = \left(\tilde{a}_\pi J_n[k_c r] + \tilde{b}_\pi Y_n[k_c r] \right) \cos[n(\theta - \theta_0)] + \left(\tilde{c}_\pi J_n[k_c r] + \tilde{d}_\pi Y_n[k_c r] \right) \sin[n(\theta - \theta_0)], \quad (135)$$

which are here characterized by eight real coefficients when $n > 0$; for $n = 0$, the $c_\pi, d_\pi, \tilde{c}_\pi, \tilde{d}_\pi$ are irrelevant and we are again left with four parameters. As in Ref. [1], we must define adapted "potential differences" that take into account the transverse symmetry of the mode profiles (Subsection IV C 2). We pose:

$$\Delta V(\theta, z, t) = V(r = a, \theta, z, t) + (-1)^m V(r = b, \theta, z, t), \quad (136)$$

$$\Delta A_z(\theta, z, t) = A_z(r = a, \theta, z, t) + (-1)^m A_z(r = b, \theta, z, t), \quad (137)$$

in which we either subtract or add up the potentials of the facing electrodes. With these, the Devoret expressions still apply with the proper angular dependence:

$$\frac{\partial \varphi(\theta, z, t)}{\partial t} = \Delta V(\theta, z, t), \quad (138)$$

$$\frac{\partial \varphi(\theta, z, t)}{\partial z} = -\Delta A_z(\theta, z, t). \quad (139)$$

The gauge fixing underlying this choice is given in Tab. IX. But there is a subtlety here: because of the high symmetry of the problem at hand, J_n and Y_n functions are both eligible in the potentials. This leads to an extra degeneracy represented by the real number α in the tabular. With our conventions, we always have $V(r = a, \theta, z, t) > 0$ while $V(r = b, \theta, z, t)$ displays the sign of $(-1)^m$. However, $|V(r = a, \theta, z, t)| \neq |V(r = b, \theta, z, t)|$ which is *different* from the TEM case discussed above, or the parallel plate result [1]. Only when $b/a \rightarrow 1$ do we recover the perfect symmetry/anti-symmetry of the electrode potentials (the same conclusions obviously apply to the A_z component). Actually, the parameter α vanishes from the expressions of the potentials on the electrodes, which is a consequence of the boundary condition. As well, the gauge invariance is relaxed as compared to the Cartesian case. As soon as:

$$a_\pi = -\frac{Y_n[k_c a] + (-1)^m Y_n[k_c b]}{J_n[k_c a] + (-1)^m J_n[k_c b]} b_\pi, \quad (140)$$

$$c_\pi = -\frac{Y_n[k_c a] + (-1)^m Y_n[k_c b]}{J_n[k_c a] + (-1)^m J_n[k_c b]} d_\pi, \quad (141)$$

and similarly for the tilded parameters, the gauge expressions Eqs. (136,137) verify the Devoret laws Eqs. (138,139). We can thus fix one constant of the pair (say a_π) as a function of the other one, which is kept unknown. In this sense, the gauge invariance is higher than in the corresponding parallel plate case [1].

TABLE IX. Gauge description for $\text{TM}_{n,m}$ waves in a coaxial waveguide with $n \geq 0, m > 0$.

Function	Expression
$A_r(r, \theta, z, t)$	$= \phi_m \frac{k_c}{2} \left(\left[\frac{(1-\alpha) [J_{n+1}(k_c r) - J_{n-1}(k_c r)]}{J_n(k_c a) + (-1)^m J_n(k_c b)} + \frac{\alpha [Y_{n+1}(k_c r) - Y_{n-1}(k_c r)]}{Y_n(k_c a) + (-1)^m Y_n(k_c b)} \right] \right. \\ \left. + \frac{a\pi}{2h_{\text{eff}}} [J_n(k_c a) [Y_{n+1}(k_c r) - Y_{n-1}(k_c r)] - [J_{n+1}(k_c r) - J_{n-1}(k_c r)] Y_n(k_c a)] \right) \cos[n(\theta - \theta_0)] \tilde{f}(z, t)$
$A_\theta(r, \theta, z, t)$	$= \phi_m \frac{n}{r} \left(\left[\frac{(1-\alpha) J_n(k_c r)}{J_n(k_c a) + (-1)^m J_n(k_c b)} + \frac{\alpha Y_n(k_c r)}{Y_n(k_c a) + (-1)^m Y_n(k_c b)} \right] \right. \\ \left. + \frac{a\pi}{2h_{\text{eff}}} [J_n(k_c r) Y_n(k_c a) - J_n(k_c a) Y_n(k_c r)] \right) \sin[n(\theta - \theta_0)] \tilde{f}(z, t)$
$A_z(r, \theta, z, t)$	$= \phi_m \beta \left(\left[\frac{(1-\alpha) J_n(k_c r)}{J_n(k_c a) + (-1)^m J_n(k_c b)} + \frac{\alpha Y_n(k_c r)}{Y_n(k_c a) + (-1)^m Y_n(k_c b)} \right] \right. \\ \left. + \frac{a\pi}{2h_{\text{eff}}} \frac{k_c^2}{\beta^2} [J_n(k_c r) Y_n(k_c a) - J_n(k_c a) Y_n(k_c r)] \right) \cos[n(\theta - \theta_0)] f(z, t)$
$V(r, \theta, z, t)$	$= \phi_m \omega \left(\frac{(1-\alpha) J_n(k_c r)}{J_n(k_c a) + (-1)^m J_n(k_c b)} + \frac{\alpha Y_n(k_c r)}{Y_n(k_c a) + (-1)^m Y_n(k_c b)} \right) \cos[n(\theta - \theta_0)] f(z, t)$
Gauge fixing	$a_\pi, \tilde{a}_\pi, c_\pi, \tilde{c}_\pi$ from Eqs. (140,141)
Gauge invariance	$b_\pi, \tilde{b}_\pi, d_\pi, \tilde{d}_\pi$ and α

3. TE modes

TE waves verify the same dispersion relation as the previous TM ones, and share the same generic symmetry. Therefore $p(r, \theta), \tilde{p}(r, \theta)$ have the same expressions.

Consider first the $n > 0$ situation. From the transverse symmetry of these modes discussed in Subsection IV C 3, we define this time:

$$\Delta V(\theta, z, t) = V(r = a, \theta, z, t) + (-1)^{m+1} V(r = b, \theta, z, t), \quad (142)$$

$$\Delta A_z(\theta, z, t) = A_z(r = a, \theta, z, t) + (-1)^{m+1} A_z(r = b, \theta, z, t). \quad (143)$$

The same arguments as in the case of TM waves apply, with Devoret relations Eqs. (138,139) leading to the results given in Tab. X. The role of the cos and sin terms in Eqs. (134,135) are simply inverted. Again, we have a degeneracy linked to the high symmetry of the problem

represented by the real number α . This time:

$$a_\pi = -\frac{Y_n[k_c a] + (-1)^{m+1} Y_n[k_c b]}{J_n[k_c a] + (-1)^{m+1} J_n[k_c b]} b_\pi, \quad (144)$$

$$c_\pi = -\frac{Y_n[k_c a] + (-1)^{m+1} Y_n[k_c b]}{J_n[k_c a] + (-1)^{m+1} J_n[k_c b]} d_\pi, \quad (145)$$

leads to the remaining gauge invariance. But as opposed to the TM situation described before, it is possible for TE waves to impose a perfect symmetry/antisymmetry $|V(r = a, \theta, z, t)| = |V(r = b, \theta, z, t)|$ and $|A_z(r = a, \theta, z, t)| = |A_z(r = b, \theta, z, t)|$ of the electrodes' potentials. This is due to the different boundary conditions applying for TE modes, and we have then:

$$\alpha = \frac{1}{2} \frac{(J_n[k_c a] - (-1)^{m+1} J_n[k_c b])(Y_n[k_c b] + (-1)^{m+1} Y_n[k_c a])}{J_n(k_c a)Y_n(k_c b) - J_n(k_c b)Y_n(k_c a)}, \quad (146)$$

which indeed would diverge for TM waves. Note that imposing this condition *is not* required by our modeling, which is why we still keep α as a gauge undefined choice in Tab. X. The gauge invariance is again larger than in the Cartesian case, see Ref. [1].

TABLE X. Gauge description for $\text{TE}_{n,m}$ modes in a coaxial waveguide, with $n > 0, m > 0$.

Function	Expression
$A_r(r, \theta, z, t)$	$= \phi_m \left(\frac{k_c}{2} \left[\frac{(1-\alpha)[J_{n+1}(k_c r) - J_{n-1}(k_c r)]}{J_n(k_c a) + (-1)^{m+1} J_n(k_c b)} + \frac{\alpha[Y_{n+1}(k_c r) - Y_{n-1}(k_c r)]}{Y_n(k_c a) + (-1)^{m+1} Y_n(k_c b)} \right] \right. \\ \left. + \frac{a}{r h_{\text{eff}}} \left[\frac{J_n[k_c r](Y_{n+1}[k_c a] - Y_{n-1}[k_c a]) - Y_n[k_c r](J_{n+1}[k_c a] - J_{n-1}[k_c a])}{(J_{n+1}[k_c a] - J_{n-1}[k_c a])Y_n[k_c a] - J_n[k_c a](Y_{n+1}[k_c a] - Y_{n-1}[k_c a])} \right] \right) \sin[n(\theta - \theta_0)] \tilde{f}(z, t)$
$A_\theta(r, \theta, z, t)$	$= \phi_m \left(-\frac{n}{r} \left[\frac{(1-\alpha)J_n(k_c r)}{J_n(k_c a) + (-1)^{m+1} J_n(k_c b)} + \frac{\alpha Y_n(k_c r)}{Y_n(k_c a) + (-1)^{m+1} Y_n(k_c b)} \right] \right. \\ \left. + \frac{k_c a}{2n h_{\text{eff}}} \left[-\frac{(J_{n+1}[k_c r] - J_{n-1}[k_c r])(Y_{n+1}[k_c a] - Y_{n-1}[k_c a])}{(J_{n+1}[k_c a] - J_{n-1}[k_c a])Y_n[k_c a] - J_n[k_c a](Y_{n+1}[k_c a] - Y_{n-1}[k_c a])} \right. \right. \\ \left. \left. + \frac{(J_{n+1}[k_c a] - J_{n-1}[k_c a])(Y_{n+1}[k_c r] - Y_{n-1}[k_c r])}{(J_{n+1}[k_c a] - J_{n-1}[k_c a])Y_n[k_c a] - J_n[k_c a](Y_{n+1}[k_c a] - Y_{n-1}[k_c a])} \right] \right) \cos[n(\theta - \theta_0)] \tilde{f}(z, t)$
$A_z(r, \theta, z, t)$	$= \phi_m \beta \left(\frac{(1-\alpha)J_n(k_c r)}{J_n(k_c a) + (-1)^{m+1} J_n(k_c b)} + \frac{\alpha Y_n(k_c r)}{Y_n(k_c a) + (-1)^{m+1} Y_n(k_c b)} \right) \sin[n(\theta - \theta_0)] f(z, t)$
$V(r, \theta, z, t)$	$= \phi_m \omega \left(\frac{(1-\alpha)J_n(k_c r)}{J_n(k_c a) + (-1)^{m+1} J_n(k_c b)} + \frac{\alpha Y_n(k_c r)}{Y_n(k_c a) + (-1)^{m+1} Y_n(k_c b)} \right) \sin[n(\theta - \theta_0)] f(z, t)$
Gauge fixing	$a_\pi, \tilde{a}_\pi, c_\pi, \tilde{c}_\pi$ from Eqs. (144,145)
Gauge invariance	$b_\pi, \tilde{b}_\pi, d_\pi, \tilde{d}_\pi$ and α

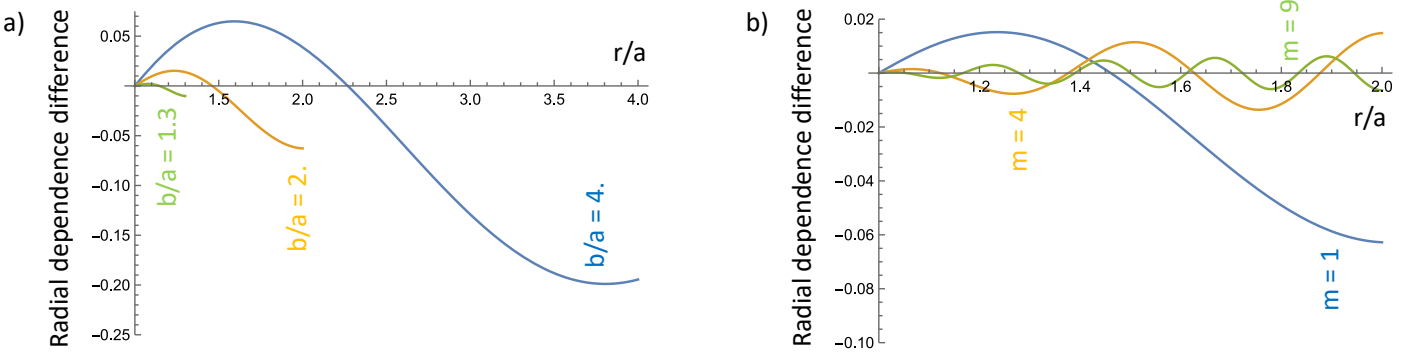


FIG. 3. Difference between the gauge profile Eq. (149) and the $g_{vir}(r)$ function (no units, to be compared to 1). a) For mode $m = 1$, different b/a ratios. b) For $b/a = 2.$, different mode numbers m . See text for details.

For the $n = 0$ waves, we must consider virtual electrodes crossing the guide with (arbitrary) azimuthal angle θ . The most natural way of extending the formalism of Ref. [1] would be to pose, for $a < r < b$:

$$\Delta V(r, z, t) = V(r, \theta, z, t) + V(r, \theta + \pi, z, t), \quad (147)$$

$$\Delta A_z(r, z, t) = A_z(r, \theta, z, t) + A_z(r, \theta + \pi, z, t). \quad (148)$$

The potentials of top and bottom parts of the virtual electrode are added up, due to the symmetry. In the gauge expressions Eqs. (134,135), only the cos terms are relevant (with four gauge coefficients to be fixed). But there is an issue here. The radial dependence created by the gauge choice writes:

$$A_z, V \propto \frac{J_0[k_c a] Y_0[k_c r] - J_0[k_c r] Y_0[k_c a]}{A'_m J_0(k_c a)}, \quad (149)$$

which is obtained by enforcing the $r = a$ boundary (at zero), and normalizing the amplitude following the same procedure as for the E_θ component (Subection III D 3), defining thus numerically A'_m . This function *is clearly different* from the $g_{vir}(r)$ one, Eq. (76). We plot the difference between these two in Fig. 3, for various ratios b/a and mode numbers m . Only when $b/a \rightarrow 1$ or $m \gg 1$ do the two expressions match; but the difference is rather

small for reasonable practical parameters (typically $< 15\%$), and one can argue that:

$$\frac{\partial \varphi(r, z, t)}{\partial t} \approx \Delta V(r, z, t), \quad (150)$$

$$\frac{\partial \varphi(r, z, t)}{\partial z} \approx -\Delta A_z(r, z, t), \quad (151)$$

can be experimentally considered as good enough, replacing the previous (and exact) Devoret expressions Eqs. (138,139). The obtained gauge is given in Tab. XI, reminding as well that Eqs. (150,151) are only approximate. This point shall be explicitly discussed in Subection V C. All coefficients are fixed, similarly to Ref. [1].

TABLE XI. Gauge description for $\text{TE}_{n=0,m}$ modes in a coaxial waveguide ($m > 0$).

Function	Expression
$A_r(r, \theta, z, t)$	$= \phi_m k_c \frac{(J_0[k_c a] Y_1[k_c r] - J_1[k_c r] Y_0[k_c a])}{A'_m J_0(k_c a)} \tilde{f}(z, t)$
$A_\theta(r, \theta, z, t)$	$= \phi_m \frac{-1}{h_{\text{eff}}} \left(\frac{2(J_1[k_c a] Y_1[k_c r] - J_1[k_c r] Y_1[k_c a])}{A_m(k_c a)} \right) \tilde{f}(z, t)$
$A_z(r, \theta, z, t)$	$= \phi_m \beta \left(\frac{J_0[k_c a] Y_0[k_c r] - J_0[k_c r] Y_0[k_c a]}{A'_m J_0(k_c a)} \right) f(z, t)$
$V(r, \theta, z, t)$	$= \phi_m \omega \left(\frac{J_0[k_c a] Y_0[k_c r] - J_0[k_c r] Y_0[k_c a]}{A'_m J_0(k_c a)} \right) f(z, t)$
Gauge fixing	$a_\pi = 0, \tilde{a}_\pi = 0, b_\pi = 0, \tilde{b}_\pi = 0 \quad (\Delta V, \Delta A_z \text{ approximate})$
Gauge invariance	None

B. Hollow cylindrical waveguide

The symmetries of the hollow cylinder are the same as for the coaxial line; so the same generic gauge expressions Eqs. (134,135) for $p(r, \theta), \tilde{p}(r, \theta)$ apply. Furthermore, there is no *a priori* reason to discard the Neumann functions Y_n , as opposed to what is discussed for the real fields \mathbf{E}, \mathbf{B} . Indeed, electric and magnetic fields must be finite everywhere, because they can be measured and directly define (after volume integration) the constants of motion. On the other hand, the potentials in our gauge fixing view are relevant *only on the electrodes*.

TABLE XII. Gauge description for $\text{TM}_{n,m}$ waves in a cylindrical hollow waveguide, $n \geq 0, m > 0$.

Function	Expression
$A_r(r, \theta, z, t)$	$= \phi_m \frac{k_c}{2} \left(+ \frac{1}{k_c a} \left[\frac{(J_{n+1}[k_c r] - J_{n-1}[k_c r])(J_{n+1}[k_c a] - J_{n-1}[k_c a])}{J_{n-1}(k_c a)^2} \right] - \frac{Y_{n-1}[k_c r] - Y_{n+1}[k_c r]}{2 Y_n[k_c a]} \right) \cos[n(\theta - \theta_0)] \tilde{f}(z, t)$
$A_\theta(r, \theta, z, t)$	$= \phi_m \frac{n}{r} \left(+ \frac{1}{k_c a} \left[\frac{J_n[k_c r](J_{n+1}[k_c a] - J_{n-1}[k_c a])}{J_{n-1}(k_c a)^2} \right] + \frac{Y_n[k_c r]}{2 Y_n[k_c a]} \right) \sin[n(\theta - \theta_0)] \tilde{f}(z, t)$
$A_z(r, \theta, z, t)$	$= \phi_m \beta \left(- \frac{k_c}{a \beta^2} \left[\frac{J_n[k_c r](J_{n+1}[k_c a] - J_{n-1}[k_c a])}{J_{n-1}(k_c a)^2} \right] + \frac{Y_n[k_c r]}{2 Y_n[k_c a]} \right) \cos[n(\theta - \theta_0)] f(z, t)$
$V(r, \theta, z, t)$	$= \phi_m \omega \left(\frac{Y_n[k_c r]}{2 Y_n[k_c a]} \right) \cos[n(\theta - \theta_0)] f(z, t)$
Gauge fixing	$b_\pi = 0, \tilde{b}_\pi = 0, d_\pi = 0, \tilde{d}_\pi = 0$
Gauge invariance	$a_\pi, \tilde{a}_\pi, c_\pi, \tilde{c}_\pi$

1. TM modes

Following the procedure presented in Ref. [1], and taking into account the symmetries of the TM waves in a hollow cylinder (Subection IV D 1), we define:

$$\Delta V(\theta, z, t) = V(r = a, \theta, z, t) + (-1)^n V(r = a, \theta + \pi, z, t), \quad (152)$$

$$\Delta A_z(\theta, z, t) = A_z(r = a, \theta, z, t) + (-1)^n A_z(r = a, \theta + \pi, z, t), \quad (153)$$

for any azimuthal position θ on the metallic guide. These "potential differences" verify Eqs. (138,139), and the corresponding gauge is given in Tab. XII. As for the coaxial line, when $n = 0$ only four gauge coefficients are relevant instead of eight. It turns out that because of the boundary condition, the functions $J_n[k_c r]$ present in the gauge expressions p, \tilde{p} vanish on the electrode: the $a_\pi, \tilde{a}_\pi, c_\pi, \tilde{c}_\pi$ are therefore undefined, which makes the gauge invariance larger than for the rectangular guide [1] (which does even not support a $n = 0$ mode, Subsection III E 1). Likewise, the $Y_n[k_c r]$ gauge functions are mandatory for the Devoret rule to apply: all potential components diverge at $r = 0$, which is acceptable since it is not part of an electrode.

TABLE XIII. Gauge description for $\text{TE}_{n,m}$ waves in a hollow cylindrical waveguide. $n > 0, m > 0$.

Function	Expression
$A_r(r, \theta, z, t)$	$= \phi_m \frac{k_c}{2} \left(\left[\frac{(1-\alpha) [J_{n+1}(k_c r) - J_{n-1}(k_c r)]}{2 J_n(k_c a)} + \frac{\alpha [Y_{n+1}(k_c r) - Y_{n-1}(k_c r)]}{2 Y_n(k_c a)} \right] \right. \\ \left. + \frac{4n^2}{r k_c^2 a} \left[\frac{J_n[k_c a] J_n[k_c r]}{(k_c a) J_n[k_c a]^2 - 2n J_n[k_c a] J_{n+1}[k_c a] + (k_c a) J_{n+1}[k_c a]^2} \right] \right) \sin[n(\theta - \theta_0)] \tilde{f}(z, t)$
$A_\theta(r, \theta, z, t)$	$= \phi_m \left(-\frac{n}{r} \left[\frac{(1-\alpha) J_n(k_c r)}{2 J_n(k_c a)} + \frac{\alpha Y_n(k_c r)}{2 Y_n(k_c a)} \right] \right. \\ \left. - \frac{n}{a} \left[\frac{J_n[k_c a] (J_{n+1}[k_c r] - J_{n-1}[k_c r])}{(k_c a) J_n[k_c a]^2 - 2n J_n[k_c a] J_{n+1}[k_c a] + (k_c a) J_{n+1}[k_c a]^2} \right] \right) \cos[n(\theta - \theta_0)] \tilde{f}(z, t)$
$A_z(r, \theta, z, t)$	$= \phi_m \beta \left(\frac{(1-\alpha) J_n(k_c r)}{2 J_n(k_c a)} + \frac{\alpha Y_n(k_c r)}{2 Y_n(k_c a)} \right) \sin[n(\theta - \theta_0)] f(z, t)$
$V(r, \theta, z, t)$	$= \phi_m \omega \left(\frac{(1-\alpha) J_n(k_c r)}{2 J_n(k_c a)} + \frac{\alpha Y_n(k_c r)}{2 Y_n(k_c a)} \right) \sin[n(\theta - \theta_0)] f(z, t)$
Gauge fixing	$a_\pi, \tilde{a}_\pi, c_\pi, \tilde{c}_\pi$ from Eqs. (154,155)
Gauge invariance	$b_\pi, \tilde{b}_\pi, d_\pi, \tilde{d}_\pi$ and α

2. TE modes

Consider first $n > 0$. In this case, real electrodes are involved and the symmetries of the modes lead for the "potential differences" $\Delta V, \Delta A$ to the same expressions as for TM waves, Eqs. (152,153). The corresponding gauge choice is given in Tab. XIII, matching the Devoret relations Eqs. (138,139). As opposed to the previous case, both $J_n[k_c r]$ and $Y_n[k_c r]$ functions within the gauge expressions p, \tilde{p} are relevant: we recover the degeneracy materialized by the angle α already discussed in the case of a coaxial line, see Subsection V A 2. The gauge invariance condition writes this time:

$$a_\pi = -\frac{Y_n[k_c a]}{J_n[k_c a]} b_\pi, \quad (154)$$

$$c_\pi = -\frac{Y_n[k_c a]}{J_n[k_c a]} d_\pi, \quad (155)$$

and similarly with tilded parameters. One can arbitrarily chose $\alpha = 0$ in order to remove the Y_n functions from the potentials, but this is not required by the modeling ($r = 0$ is not part of an electrode). We find out that the gauge invariance is again larger than for its

Cartesian (rectangular guide) counterpart [1].

As for the coaxial guide, the TE $n = 0$ modes deal with virtual electrodes. In the latter case, we could define approximate Eqs. (150,151) restoring somehow our intuitive expectations for "Devoret-like" relationships. For the hollow cylinder, *this is definitely impossible*. In our gauge choice, we must discard the Y_0 function because the $r = 0$ position is part of our virtual electrode. We are left with a single gauge coefficient \tilde{a}_π which cannot be fixed in a convenient way if we follow strictly the previous method, as can be seen in Tab. XIV. We must conclude that there is something very peculiar about these $\text{TE}_{0,m}$ modes, which have no equivalent in the Cartesian geometry (see Subsection III E 2). This deserves to be analyzed, and it is the purpose of the following Subsection.

TABLE XIV. Gauge description for $\text{TE}_{n=0,m}$ modes in a hollow cylindrical waveguide ($m > 0$).

Function	Expression
$A_r(r, \theta, z, t)$	$= -\tilde{a}_\pi k_c J_1[k_c r] \tilde{f}(z, t)$
$A_\theta(r, \theta, z, t)$	$= \phi_m \frac{-1}{h_{\text{eff}}} \left(\frac{2J_1[k_c r]}{A_m} \right) \tilde{f}(z, t)$
$A_z(r, \theta, z, t)$	$= -\tilde{a}_\pi \beta J_0[k_c r] f(z, t)$
$V(r, \theta, z, t)$	$= -\tilde{a}_\pi \omega J_0[k_c r] f(z, t)$
Gauge fixing	$a_\pi = 0, \quad b_\pi = 0, \quad \tilde{b}_\pi = 0$
Gauge invariance	$\tilde{a}_\pi \quad (\Delta V, \Delta A_z \text{ incompatible, see text})$

C. Gauge fixing strategies: Cartesian vs cylindrical geometries

Section IV presented the procedure recasting all physical quantities in terms of the variable φ . Choosing a reference electrode when the transmission line has non-equivalent surfaces (coaxial case), a lengthscale h_{eff} is introduced. The formalization is then *unique*. However, from the preceding Section it appears that linking this φ to the potentials \mathbf{A}, V is *not*

straightforward. The strategy of Ref. [1] had been constructed from the generalized flux concept first proposed by Devoret in Ref. [2] for quantum circuits:

$$\varphi(t) = \int_{-\infty}^t \Delta V(t') dt', \quad (156)$$

where ΔV is the voltage drop between two nodes. The fluxes φ and their conjugate variables, the branch charges Q , are all we need to describe the quantum circuit. Surplus variables are eliminated using Kirchhoff's laws, and the remaining φ, Q pairs enable to write an Hamiltonian for the whole circuit. These constitute the system's degrees of freedom which must be quantized, following conventional recipes [2].

The basic assumption of circuit theory is that each part defined by two nodes can be considered as a *lumped element* (it is much smaller than the relevant signal's wavelength). This enables to write $\Delta V = \int \mathbf{E} \cdot d\mathbf{s}$ across it, independently of the integration path [2, 16]. This is extremely convenient from an engineering point of view: the quasi-static type solutions of Maxwell's equations lead to the well-known circuit analysis toolbox [16]. The voltage ΔV is a well-defined measurable quantity, just like the current I flowing through the branch; and they characterize perfectly its state [2].

By definition, a transmission line *is not* a lumped element. But if one considers only TEM transport confined within two conductors (say *elec. 1* and *elec. 2*), the situation remains fairly simple: the transverse fields verify Laplace's equation, which means that exactly like in the static case we can derive them from a scalar potential Φ . The quantity $\Delta\Phi = \Phi(\text{elec. 1}) - \Phi(\text{elec. 2}) = \int \mathbf{E} \cdot d\mathbf{s}$ is again independent of the path: this is what engineers *define* as being the voltage difference [16]. Very conveniently, we end up with a formalism compatible with circuit theory for $\Delta\Phi$, which can be easily quantized, and travels in the guide according to a d'Alembert equation [6, 16].

But strictly speaking, this quantity $\Delta\Phi$ can be identified to ΔV *only* when imposing a longitudinal gauge. Eq. (156) can then be recast in:

$$\left\{ \begin{array}{l} \partial\varphi/\partial t = \Delta V, \\ \partial\varphi/\partial z = -\Delta A_z, \end{array} \right. \quad (157)$$

with the second equivalent equation being a consequence of the Lorenz gauge, Eq. (126). ΔA_z is defined as $A_z(\text{elec. 1}) - A_z(\text{elec. 2})$, exactly like we have $\Delta V = V(\text{elec. 1}) - V(\text{elec. 2})$. But what about non-TEM waves? What has been demonstrated in Ref. [1]

is that for a Cartesian geometry, one can *always* find a gauge that fulfills these relationships, for each TEM, TM and TE traveling solution. The "potential differences" must be generalized, taking into account the transverse symmetry of the \mathbf{E}, \mathbf{B} fields:

$$\Delta V(\eta, z, t) = V(\{\eta\} \in \text{elec. 1}, z, t) + \sigma_z V(\{\eta\} \in \text{elec. 2}, z, t), \quad (158)$$

$$\Delta A_z(\eta, z, t) = A_z(\{\eta\} \in \text{elec. 1}, z, t) + \sigma_z A_z(\{\eta\} \in \text{elec. 2}, z, t), \quad (159)$$

with $\sigma_z \in \{\pm 1\}$ a "parity coefficient" [1]. η represents the transverse coordinate running along an electrode (and symmetrically along the other one), parametrized from $\{x, y\}$ for Cartesian. Therefore in general, the voltage drop ΔV depends on η , which was not the case for TEM waves. This approach has been our starting point in the preceeding Sections.

It turns out that another gauge equation can be matched, for *any type* of traveling solution in the Cartesian waveguides:

$$\frac{1 + \mathcal{K}}{h_{\text{eff}}} \varphi = -\Delta A_{\mathbf{n}}, \quad (160)$$

with \mathcal{K} a coefficient related to the electrodes' geometry. We obtain $\mathcal{K} = 1$ for both parallel plates and rectangular guides. The quantity $\Delta A_{\mathbf{n}}$ is then defined as:

$$\Delta A_{\mathbf{n}}(\eta, z, t) = \mathbf{n} \cdot \mathbf{A}(\{\eta\} \in \text{elec. 1}, z, t) + \sigma_{\mathbf{n}} \mathbf{n} \cdot \mathbf{A}(\{\eta\} \in \text{elec. 2}, z, t), \quad (161)$$

with \mathbf{n} the normal to the electrode's surface, and $\sigma_{\mathbf{n}} \in \{\pm 1\}$. For this quantity, the symmetry coefficient $\sigma_{\mathbf{n}}$ is actually the same as for the charges and currents. This "transverse" gauge feature had not been pointed out in Ref. [1].

Remarkably, each TEM, TM and TE mode of the cylindrical geometry supports as well a gauge that verifies the rule Eq. (160). For the fully symmetric hollow pipe, we again have $\mathcal{K} = 1$ (for all wave types, including the TE $n = 0$ one). In the case of the coaxial guide, we obtain $0 < \mathcal{K} < 1$:

$$\text{TEM: } \mathcal{K} = \frac{a}{b}, \quad (162)$$

$$\text{TM: } \mathcal{K} = \frac{a}{b} \frac{\pi}{2} \left| Y_n(k_c a) [(k_c b) J_{n-1}(k_c b) - n J_n(k_c b)] - J_n(k_c a) [(k_c b) Y_{n-1}(k_c b) - n Y_n(k_c b)] \right|, \quad (163)$$

$$\text{TE } (n \neq 0): \mathcal{K} = \frac{a}{b} \frac{\pi}{2} \left| J_n(k_c b) [n Y_n(k_c a) - (k_c a) Y_{n-1}(k_c a)] - Y_n(k_c b) [n J_n(k_c a) - (k_c a) J_{n-1}(k_c a)] \right|. \quad (164)$$

For the TE $n = 0$ coaxial waves, we get $\mathcal{K} = 1$; this intuitively matches the fact that the virtual electrodes are perfectly symmetric. Taking the limit $b/a \rightarrow 1$, we recover the parallel plate results with $\mathcal{K} \rightarrow 1$.

The key property is that for *all modes that do not involve virtual electrodes*, there exists a gauge transformation that swaps the potentials from matching Eq. (160) to matching Eq. (157). It is then perfectly lawful to use Devoret's expressions Eq. (157) to describe the dynamics of the fields, in agreement with conventional electronics (which is precisely what we did in the previous Subsections). Interestingly, the gauge that verifies Eq. (160) also brings in:

$$\Delta V = 0, \quad (165)$$

$$\Delta A_z = 0. \quad (166)$$

If this is a fundamental property, it is outside of our scope, and shall be addressed elsewhere. This symmetry *is broken* for the TE $n = 0$ modes, the ones which require virtual electrodes to be defined. Pleasantly enough, for the parallel plate guide the two gauge rules can be satisfied simultaneously [1]: Eq. (160) is always true, and one can conveniently chose a gauge that also matches Eq. (157). The point is that *this is impossible* for the TE $n = 0$ waves traveling in a cylindrical geometry, as demonstrated in Section V. If this contains some fundamental meaning is again outside of our scope.

How shall we deal with these pathological TE $n = 0$ traveling waves? There is a very simple, and pragmatic answer. The Devoret relations Eq. (157), together with the definitions of surface charges σ_s and currents \mathbf{j}_s (s being any electrode) found in Section IV lead to:

$$q \propto \Delta V, \quad (167)$$

$$I \propto \Delta A_z, \quad (168)$$

with q a charge per unit length and I a longitudinal current, obtained by integration of σ_s and $\mathbf{j}_s \cdot \mathbf{z}$ over a proper transverse dimension. The point is that q and I are *physical measurable quantities* (actually the ones transported in the transmission line): this means that this gauge choice turns the somehow abstract quantities $\Delta V, \Delta A_z$ into sensible objects. And from an engineering point of view, this is all we need; when one deals with a voltage in a circuit, by no means do we directly refer to a gauge property. But what is essential, is

TABLE XV. Definition of the "potential differences" for each configuration encountered in a cylindrical geometry. The gauge property is reminded (last column), and $\sigma_{\mathbf{n}}$ is also the symmetry coefficient of charges/currents, see text for details.

Wave type	"Potential differences"	Symmetry properties
TEM	$\Delta V(z, t) = V(r = a, z, t) + \sigma_z V(r = b, z, t)$	Transform trans./long.
	$\Delta A_z(z, t) = A_z(r = a, z, t) + \sigma_z A_z(r = b, z, t)$	$\sigma_z = -1$
	$\Delta A_{\mathbf{n}}(z, t) = A_r(r = a, z, t) - \sigma_{\mathbf{n}} A_r(r = b, z, t)$	$\sigma_{\mathbf{n}} = -1$
TM _{n,m}	$\Delta V(\theta, z, t) = V(r = a, \theta, z, t) + \sigma_z V(r = b, \theta, z, t)$	Transform trans./long.
	$\Delta A_z(\theta, z, t) = A_z(r = a, \theta, z, t) + \sigma_z A_z(r = b, \theta, z, t)$	$\sigma_z = +(-1)^m$
	$\Delta A_{\mathbf{n}}(\theta, z, t) = A_r(r = a, \theta, z, t) - \sigma_{\mathbf{n}} A_r(r = b, \theta, z, t)$	$\sigma_{\mathbf{n}} = -(-1)^m$
TE _{$n \neq 0, m$}	$\Delta V(\theta, z, t) = V(r = a, \theta, z, t) + \sigma_z V(r = b, \theta, z, t)$	Transform trans./long.
	$\Delta A_z(\theta, z, t) = A_z(r = a, \theta, z, t) + \sigma_z A_z(r = b, \theta, z, t)$	$\sigma_z = +(-1)^{m+1}$
	$\Delta A_{\mathbf{n}}(\theta, z, t) = A_r(r = a, \theta, z, t) - \sigma_{\mathbf{n}} A_r(r = b, \theta, z, t)$	$\sigma_{\mathbf{n}} = -(-1)^{m+1}$
TE _{$n=0, m$}	$\Delta V_{\text{eff}}(r, z, t) = \phi_m \omega g_{vir}(r) f(z, t)$	Only transverse
	$\Delta A_z \text{eff}(r, z, t) = \phi_m \beta g_{vir}(r) f(z, t)$	$\sigma_z = +1$
	$\Delta A_{\mathbf{n}}(r, z, t) = A_{\theta}(r, \theta, z, t) - \sigma_{\mathbf{n}} A_{\theta}(r, \theta + \pi, z, t)$	$\sigma_{\mathbf{n}} = -1$
TM _{n,m}	$\Delta V(\theta, z, t) = V(r = a, \theta, z, t) + \sigma_z V(r = a, \theta + \pi, z, t)$	Transform trans./long.
	$\Delta A_z(\theta, z, t) = A_z(r = a, \theta, z, t) + \sigma_z A_z(r = a, \theta + \pi, z, t)$	$\sigma_z = +(-1)^n$
	$\Delta A_{\mathbf{n}}(\theta, z, t) = -A_r(r = a, \theta, z, t) - \sigma_{\mathbf{n}} A_r(r = a, \theta + \pi, z, t)$	$\sigma_{\mathbf{n}} = -(-1)^{n+1}$
TE _{$n \neq 0, m$}	$\Delta V(\theta, z, t) = V(r = a, \theta, z, t) + \sigma_z V(r = a, \theta + \pi, z, t)$	Transform trans./long.
	$\Delta A_z(\theta, z, t) = A_z(r = a, \theta, z, t) + \sigma_z A_z(r = a, \theta + \pi, z, t)$	$\sigma_z = +(-1)^n$
	$\Delta A_{\mathbf{n}}(\theta, z, t) = -A_r(r = a, \theta, z, t) - \sigma_{\mathbf{n}} A_r(r = a, \theta + \pi, z, t)$	$\sigma_{\mathbf{n}} = -(-1)^{n+1}$
TE _{$n=0, m$}	$\Delta V_{\text{eff}}(r, z, t) = \phi_m \omega g_{vir}(r) f(z, t)$	Only transverse
	$\Delta A_z \text{eff}(r, z, t) = \phi_m \beta g_{vir}(r) f(z, t)$	$\sigma_z = +1$
	$\Delta A_{\mathbf{n}}(r, z, t) = A_{\theta}(r, \theta, z, t) - \sigma_{\mathbf{n}} A_{\theta}(r, \theta + \pi, z, t)$	$\sigma_{\mathbf{n}} = -1$

that this potential *is an image* of the charges and currents flowing in the circuit, which is exactly what Eqs. (167,168) guarantee. The natural solution to handling TE $n = 0$ modes is therefore to *impose* in the Devoret equations an effective voltage ΔV_{eff} (and longitudinal potential $\Delta A_{z\text{ eff}}$) which is $\propto A_\theta$. This physically means that we actually "swap our gauge", but keep all the useful properties of the conventional formalism. These effective potentials are defined on the virtual electrodes, so they correspond to charges/currents *that would be excited if one would use a non-invasive electrode* to detect them. At the same time, the "real voltage" ΔV (and ΔA_z) on the real electrodes *can be set to zero*, since it is a valid gauge choice (see e.g. Tab. XIV; this is true for any of the other TE $n = 0$ situations). The outcomes of this Subsection are summarized in Tab. XV.

VI. FIELD QUANTIZATION

We shall now quantize the X and Y quadratures, following strictly the method of Ref. [1]. To start with, let us define:

$$\varphi_{\text{max}}(z, t) = \phi_m \tilde{f}(z, t), \quad (169)$$

which is nothing but the amplitude of the φ functions without the $g_{\text{real}}, g_{\text{vir}}$ transverse dependencies, Eqs. (35,36). Integrating H (energy) and \mathbf{P} (momentum) over the transverse direction (the $a d\theta$ periphery or the virtual plane) leads to:

$$H = \int_{z=0}^L \left[\frac{1}{2} C_H^{-1} \left(C_H \frac{\partial \varphi_{\text{max}}(z, t)}{\partial t} \right)^2 + \frac{1}{2} L_H^{-1} \left(\frac{\partial \varphi_{\text{max}}(z, t)}{\partial z} \right)^2 + \frac{1}{2} C_P (c k_c)^2 \varphi_{\text{max}}(z, t)^2 \right] dz / L, \quad (170)$$

$$\mathbf{P} = \int_{z=0}^L \left[\left(C_P \frac{\partial \varphi_{\text{max}}(z, t)}{\partial t} \right) \left(-\frac{\partial \varphi_{\text{max}}(z, t)}{\partial z} \right) \right] dz / L \mathbf{z}, \quad (171)$$

for *all configurations* discussed here. This writing is strictly the same as the one of Cartesian guides [1], and the obtained coefficients are listed in Tab. XVI (together with a reminder of other mode-dependent quantities). The velocity appearing in this tabular is the one that enters the φ propagation equation, together with k_c . Remember that only for TEM waves do we have $v_\phi = c$; for both TM and TE solutions, the phase velocity verifies $v_\phi = c k / |\beta| \neq c$. C_H and C_P are total capacitances (in F) while L_H is a "total inductance" (actually in H/m²),

characteristic of each mode. The proper mode inductance writes L_H/β^2 , and arises from the $\partial\varphi_{max}/\partial z$ that appears in Eq. (170). Finally, we introduce:

$$Q_{max}(z, t) = +C_P \frac{\partial\varphi_{max}(z, t)}{\partial t}, \quad (172)$$

the charge amplitude (in Coulomb) that propagates along with $\varphi_{max} \propto \tilde{f}[z, t]$ (in quadrature, with a $f[z, t]$ dependence).

We now promote the two quadratures to operators ($X \rightarrow \hat{X}$, $Y \rightarrow \hat{Y}$). Performing the last integration over z we obtain:

$$\hat{H} = (2 C_P \omega \phi_m^2) \omega \left(\frac{\hat{X}^2 + \hat{Y}^2}{4} \right), \quad (173)$$

$$\hat{\mathbf{P}} = (2 C_P \omega \phi_m^2) \beta \left(\frac{\hat{X}^2 + \hat{Y}^2}{4} \right) \mathbf{z}. \quad (174)$$

The generalized flux and charge operators therefore obey the commutation relation:

$$[\hat{\varphi}_{max}(z, t), \hat{Q}_{max}(z, t)] = (2 C_P \omega \phi_m^2) \frac{[\hat{X}, \hat{Y}]}{2}. \quad (175)$$

These can be conveniently re-expressed in terms of the creation/annihilation operators \hat{b}^\dagger, \hat{b} :

$$\hat{X} = \hat{b}^\dagger + \hat{b}, \quad \hat{Y} = i(\hat{b}^\dagger - \hat{b}), \quad (176)$$

which straightforwardly lead to:

$$[\hat{X}, \hat{Y}] = 2i[\hat{b}, \hat{b}^\dagger], \quad (177)$$

$$\hat{X}^2 + \hat{Y}^2 = 4 \left(\hat{b}^\dagger \hat{b} + \frac{[\hat{b}, \hat{b}^\dagger]}{2} \right). \quad (178)$$

Technically, \hat{b}, \hat{b}^\dagger are implicitly $t = 0$ operators, in a Heisenberg picture [2]. Their time-evolved expressions are obviously $\hat{b} e^{-i\omega t}$ and $\hat{b}^\dagger e^{+i\omega t}$ respectively, which lead to the time-dependence of the f, \tilde{f} functions. We recover textbook formulations by imposing:

$$2 C_P \omega \phi_m^2 = \hbar, \quad (179)$$

$$[\hat{b}, \hat{b}^\dagger] = 1, \quad (180)$$

which *fundamentally* link our field amplitude E_m (hidden in ϕ_m) to Planck's reduced constant \hbar , and defines our modes as being *bosons*. More details and mathematical properties can be

found in Ref. [1]. In particular, quantum mechanics enables to understand the cutoff energy of TM waves:

$$\Delta_c = \hbar \omega_c, \quad (181)$$

as being an energy gap per photon, needed to launch the wave. Similarly for TE waves:

$$m c^2 = \hbar \omega_c, \quad (182)$$

where m is an effective photon mass, appearing in the Klein-Gordon equation.

TABLE XVI. Modal coefficients C_H , C_P , L_H (together with k_c and the velocity appearing in the Klein-Gordon equation). We remind that $C_d = \epsilon/h_{\text{eff}}$ and $Ld^{-1} = 1/(\mu h_{\text{eff}})$. $k_c \neq 0$ and h_{eff} are given in the core of the text. We define $\gamma[n] = 1$ for $n = 0$ and $\gamma[n] = 2$ for $n \neq 0$. Note that non-TEM waves have the same writing in coaxial and hollow cylinder guides.

Wave type	Modal coefficients	Potential-related parameters
	$C_H = C_d (2\pi a) L$	
TEM , coaxial	$C_P = C_H$	$k_c = 0$, K-G velocity c
	$L_H^{-1} = L_d^{-1} (2\pi a) L$	
	$C_H = C_d (2\pi a/\gamma[n]) L$	
TM _{n,m} , coaxial	$C_P = C_H (k/\beta)^2$	$k_c \neq 0$, K-G velocity v_ϕ
	$L_H^{-1} = L_d^{-1} (k/\beta)^4 (2\pi a/\gamma[n]) L$	
	$C_H = C_d (2\pi a/\gamma[n]) L$	
TE _{n,m} , coaxial	$C_P = C_H$	$k_c \neq 0$, K-G velocity c
	$L_H^{-1} = L_d^{-1} (2\pi a/\gamma[n]) L$	
	$C_H = C_d (2\pi a/\gamma[n]) L$	
TM _{n,m} , cylinder	$C_P = C_H (k/\beta)^2$	$k_c \neq 0$, K-G velocity v_ϕ
	$L_H^{-1} = L_d^{-1} (k/\beta)^4 (2\pi a/\gamma[n]) L$	
	$C_H = C_d (2\pi a/\gamma[n]) L$	
TE _{n,m} , cylinder	$C_P = C_H$	$k_c \neq 0$, K-G velocity c
	$L_H^{-1} = L_d^{-1} (2\pi a/\gamma[n]) L$	

VII. CONCLUSION

We report on the canonical quantization of electromagnetic fields in cylindrical waveguides, adapting the formalism already developed for Cartesian geometries [1]. We identify the generalized flux φ and its conjugate charge Q that enable to recast all the field's properties. The theory invokes a gauge fixing required to deduce φ from the potentials \mathbf{A}, V , which must be a fundamental property *for all types of waves*, namely TEM, TM and TE. We discuss how this can be recast in "potential differences" $\Delta V, \Delta A_z$, producing "Devoret relationships" particularly relevant for quantum engineering [2, 6]. The conclusions reached in Ref. [1] also apply here, especially the introduction of "virtual electrodes", but with some specificities linked to the higher symmetry of the problem at hand.

Exactly like in the Cartesian case, the cutoff frequency ω_c appears as a consequence of an energy gap for TM waves, and of a photon mass for TE. Modal parameters C_H, C_P and L_H are introduced, leading to expressions for energy H and momentum \mathbf{P} identical to those of Ref. [1]. These results are robust, even though extra modes are allowed in the coaxial configuration as compared to the parallel plate guide (all $n \neq 0$ modes), and TM $n = 0$ waves do exist in the hollow cylinder (but not in a rectangular guide).

Beyond all similarities, the comparison cylinder/square is particularly enlightening *because of the peculiarities* encountered here. The potentials considered in this work can diverge at $r = 0$ with no physical relevance, while this is impossible in a Cartesian geometry. For all waves supported by real electrodes, we pointed out the existence of a gauge transformation that links φ to the *transverse* potential difference $\Delta A_{\mathbf{n}}$, and at the same time generates $\Delta A_z = \Delta V = 0$. On the other hand, the TE $n = 0$ modes which require virtual electrodes to be described, *do not support* this transformation and seem in this sense quite special. If these facts bear a fundamental meaning remains an open question, and might be investigated in the future.

An important outcome of the model is the capability to define capacitance and inductance densities *for all types of modes* TEM, TM and TE, which makes the link with conventional wave propagation: the well known *telegrapher's equation*. How to formalize this, in particular in the framework of the quantum input-output theory [5] shall be left for future works.

The present formalism shall be extended to other types of guides. Especially, the *bifilar* geometry (hosting only TEM modes), and the coplanar waveguide (hosting quasi-TEM)

which is heavily used in quantum engineering. Both have their specificity which might require some adaptations of the reasoning: the former corresponds to an open geometry, while the latter involves multiple electrodes which do not share a common symmetry. As well, dielectric interfaces have not been addressed at all; in particular, how shall we deal with *hybrid waves*, which have both an E_z and B_z component? This would open the way to generalizations in even more complex media, e.g. structured photonic environments [21] and multimode quantum networks [11].

ACKNOWLEDGEMENTS

This work is a follow-up of a previous article, Ref. [1]. We are thankful to the European Microkelvin Platform community (EMP), for strong support over the years. We also wish to acknowledge useful interactions among the participants of the former "Groupement de Recherche MecaQ".

DATA AVAILABILITY

No data was used or created for this manuscript. A Mathematica[®] code is available at the following URL: <https://cloud.neel.cnrs.fr/index.php/s/CnnYPKn8XHYZgXa>.

CONFLICT OF INTEREST

The authors have no conflicts to disclose.

- [1] E. Collin and A. Delattre, *New J. Phys.* **27**, 093502 (2025).
- [2] M. H. Devoret, *Les Houches, Session LXIII* (1997).
- [3] C. Cohen-Tannoudji, J. Dupont-Roc, and G. Grynberg, *Photons and Atoms: Introduction to Quantum Electrodynamics* (Wiley, 1989).
- [4] R. Loudon, *The Quantum Theory of Light*, 3rd ed. (Oxford University Press, 2000).
- [5] C. W. Gardiner and P. Zoller, *Quantum Noise* (Springer, 2004).

- [6] A. A. Clerk, M. H. Devoret, S. M. Girvin, F. Marquardt, and R. J. Schoelkopf, Rev. Mod. Phys. **82**, 1155 (2010).
- [7] U. Vool and M. Devoret, International Journal of Circuit Theory and Applications **45**, 897 (2017).
- [8] M. H. Devoret and R. J. Schoelkopf, Science **339**, 1169 (2013).
- [9] A. Blais, R.-S. Huang, A. Wallraff, S. M. Girvin, and R. J. Schoelkopf, Phys. Rev. A **69**, 062320 (2004).
- [10] A. Blais, A. L. Grimsmo, S. M. Girvin, and A. Wallraff, Rev. Mod. Phys. **93**, 025005 (2021).
- [11] M. F. Gely, A. Parra-Rodriguez, D. Bothner, Y. M. Blanter, and G. A. Steele, Phys. Rev. B **95**, 245115 (2017).
- [12] C. Macklin, K. O'Brien, D. Hover, M. E. Schwartz, V. Bolkhovsky, X. Zhang, W. D. Oliver, and I. Siddiqi, Science **350**, 307 (2015).
- [13] T. C. White, K. P. O'Brien, and I. Siddiqi, Nature Reviews Physics **5**, 87 (2023).
- [14] R. E. Collin, *Field Theory of Guided Waves*, 2nd ed. (IEEE Press, 1990).
- [15] J. D. Jackson, *Classical Electrodynamics*, 3rd ed. (Wiley, 1999).
- [16] D. M. Pozar, *Microwave Engineering*, 4th ed. (Wiley, 2011).
- [17] H. Padamsee, J. Knobloch, and T. Hays, *RF Superconductivity for Accelerators* (Wiley-VCH, 1998).
- [18] M. Aspelmeyer, T. J. Kippenberg, and F. Marquardt, Rev. Mod. Phys. **86**, 1391 (2014).
- [19] C. A. Regal, J. D. Teufel, and K. W. Lehnert, Nature Physics **4**, 555 (2008).
- [20] G. Kurizki, P. Bertet, Y. Kubo, K. Mølmer, D. Petrosyan, P. Rabl, and J. Schmiedmayer, PNAS **112**, 3866 (2015).
- [21] T. Ozawa, H. M. Price, A. Amo, N. Goldman, M. Hafezi, L. Lu, M. C. Rechtsman, D. Schuster, J. Simon, O. Zilberberg, and I. Carusotto, Rev. Mod. Phys. **91**, 015006 (2019).
- [22] M. Abramowitz and I. A. Stegun, *Handbook of Mathematical Functions with Formulas, Graphs, and Mathematical Tables* (National Bureau of Standards, Washington, D.C., 1964) reprinted by Dover Publications, New York, 1965.
- [23] F. W. J. Olver, D. W. Lozier, R. F. Boisvert, and C. W. Clark, *NIST Handbook of Mathematical Functions* (Cambridge University Press, Cambridge, UK, 2010) print companion to the NIST Digital Library of Mathematical Functions.

[24] G. B. Arfken, H. J. Weber, and F. E. Harris, *Mathematical Methods for Physicists: A Comprehensive Guide*, 7th ed. (Academic Press, Oxford, UK, 2013).